Defect-driven flexochemical coupling in thin ferroelectric films

Eugene A. Eliseev, Ivan S. Vorotiahin, Yevhen M. Fomichov, Maya D. Glinchuk, Sergei V. Kalinin, Yuri A. Genenko, and Anna N. Morozovska

Phys. Rev. B **97**, 024102 — Published 5 January 2018

DOI: 10.1103/PhysRevB.97.024102

Defect driven flexo-chemical coupling in thin ferroelectric films

Eugene A. Eliseev,[1] Ivan. S. Vorotiahin[2, 3], Yevhen M. Fomichov [1,4], Maya D. Glinchuk[1], Sergei V. Kalinin[5], Yuri A. Genenko[3*], and Anna N. Morozovska[2†]

[1]Institute for Problems of Materials Science, National Academy of Sciences of Ukraine, 3, Krjijanovskogo, 03142 Kyiv, Ukraine

[2]Institute of Physics, National Academy of Sciences of Ukraine, 46, Prospekt Nauky, 03028 Kyiv, Ukraine

[3] Institut für Materialwissenschaft, Technische Universität Darmstadt, Otto-Berndt-Str. 3, 64287 Darmstadt, Germany

[4] Faculty of Mathematics and Physics, Charles University, V Holesovickach 2, 18000 Prague 8, Czech Republic

[5] The Center for Nanophase Materials Sciences, Oak Ridge National Laboratory, Oak Ridge, TN 37831

Abstract

Using Landau-Ginzburg-Devonshire theory, we considered the impact of the flexoelectro-chemical coupling on the size effects in polar properties and phase transitions of thin ferroelectric films with a layer of elastic defects. We investigated a typical case, when defects fill a thin layer below the top film surface with a constant concentration creating an additional gradient of elastic fields. The defective surface of the film is not covered with an electrode, but instead with an ultra-thin layer of ambient screening charges, characterized by a surface screening length. This geometry is typical for the scanning probe piezoelectric force microscopy.

Obtained results revealed an unexpectedly strong effect of the joint action of Vegard stresses and flexoelectric effect (shortly flexo-chemical coupling) on the ferroelectric transition temperature, distribution of the spontaneous polarization and elastic fields, domain wall structure and period in thin $PbTiO_3$ films containing a layer of elastic defects. A nontrivial result is the ferroelectricity persistence at film thicknesses below 4 nm, temperatures lower than 350 K and relatively high surface screening length (~0.1 nm). The origin of this phenomenon is the flexoelectric coupling leading to the re-building of the domain structure in the film (namely the cross-over from c-domain stripes to a-type closure domains) when its thickness decreases below 4 nm. The ferroelectricity persistence is facilitated by negative Vegard effect. For positive Vegard effect, thicker films exhibit the appearance of pronounced maxima on the thickness dependence of the transition temperature, whose position and height can be controlled by the defect type and concentration. The revealed features may have important implications for miniaturization of ferroelectric-based devices.

[*] Corresponding author 2. E-mail: genenko@mm.tu-darmstadt.de
[†] Corresponding author 1. E-mail: anna.n.morozovska@gmail.com

I. INTRODUCTION

Deep physical understanding and a possible control of the thin ferroelectric films polar properties are important for both fundamental research and the most promising applications in memory elements as well as many other devices [1]. With decreasing the film thickness its ferroelectric properties usually decline until their complete disappearance at thicknesses smaller than the critical one [2]. Feasible ways to avoid the size-induced phase transition in thin epitaxial films are, for example, selecting of an appropriate substrate [3] or modification of their chemical composition [4]. Particularly it was shown that the retaining of ferroelectricity down to ultrathin films (3 – 5 lattice constants thick) is provided by the "self-polarizing" role of elastic strains arising in the film due to mismatching lattice constants of the film and the substrate [5]. Earlier it was shown by Roytburd et al. [6] that the change in the polarization is proportional to internal stresses due to film-substrate misfit strain, and, as an example, a significant recovery in the piezoelectric constant and susceptibility in $PbZr_{0.2}Ti_{0.8}O_3$ films on (001) $LaAlO_3$ substrate was revealed.

The presence of point elastic defects (such as uncharged impurities and vacancies, elastic dipoles, dilatation centers [7]) can strongly impact the electric polarization of films via electrostriction [8], flexoelectric effect (see e.g. [9, 10, 11, 12, 13]) and "chemical" strains, or Vegard stresses (see e.g. [14, 15, 16, 17, 18, 19]). Actually, when the chemical heterogeneity is the actual mechanism for strain, the generalized Hooke's law relates the defect concentration excess δN, elastic stress tensor σ_{ij} and strain tensor u_{ij} in accordance with the Vegard law [16 - 19], $\sigma_{ij} = W_{ij}\ \delta N + c_{ijkl}u_{kl}$. Due to the gradient nature, the elastic defect influence is much more complex and less studied than the effect of homogeneous elastic strains arising in a film due to the film and substrate lattice mismatch [20]. A joint action of Vegard stresses and flexoelectric effect, named **flexo-chemical effect** [21], can explain some unusual phenomena caused by size effects, such as e.g. reentrant ferroelectric phase with enhanced polarization at room temperature observed in $BaTiO_3$ nanoparticles with sizes less than 20 nm [22].

Flexoelectric effect, chemical composition gradient and/or defect impact on the polar properties of ferroelectric thin films were studied theoretically by several authors, but mostly these three different effects have been studied separately [see the columns "Flexoelectric effect" and "Composition gradient, defects" in **Table I**]. For instance, Marvan et al. [23] evolved the theory of compositionally graded ferroelectrics.

Roytburd and Slutsker [24] proposed a phenomenological model of a graded ferroelectric film taking into account approximate expressions for depolarization field containing the term proportional to the average polarization, similar to the one proposed earlier by Kretschmer and Binder [25]. In the subsequent papers they applied the same method to the ferroelectric films with domains [26, 27]. Note

that the approximation for the depolarization field being undoubtedly useful for approximate analytical results derivation in a single-domain case, becomes questionable in a poly-domain case. For the rigorous consideration of domains appearance one should solve numerically the coupled problem containing in Poisson equation for the electric field and nonlinear equation for polarization dependence on the field [23]. The coupled problem is typically solved by a self-consistent phase field method allowing modeling of very complex domain structures such as flux-closure domains [28] and domain vortexes [29, 30, 31] in thin ferroelectric films and superlattices.

Bratkovsky and Levanyuk [32] theoretically studied the smearing of phase transition due to a surface effect or a bulk inhomogeneity in single-domain ferroelectric nanostructures. Ban et al. [33] and Zhong et al. [34] established the theoretical fundamentals of graded ferroic materials piezoelectric and polar responses. Morozovska et al. [35] studied theoretically the domain wall interaction with elastic defects in uniaxial ferroelectrics. The papers [23-35] considered chemical composition gradient only and ignored the flexocoupling. Other authors considered only the impact of flexocoupling on the thermodynamics and kinetics of polarization reversal in thin ferroelectric film (see e.g. Vorotiahin et al. [36, 37]).

Remarkably the separate theoretical consideration of the flexoelectric coupling and inhomogeneous strains in thin ferroelectric films leads to the results, which can be oversimplified for realistic applications, because the flexocoupling is omnipresent and its relative contribution significantly increases with the film thickness decrease [13]. However there are only a few theoretical studies considering both flexoelectric and chemical composition gradient effects, all of which are some particular cases [see **Table I**]. For instance, Catalan et al. [38] studied the effect of flexoelectricity on the polar and dielectric properties of inhomogeneously strained ferroelectric thin films. Karthik et al. [39] revealed giant built-in electric fields due to flexoelectricity in compositionally graded ferroelectric thin films. Morozovska et al. [40] studied the flexocoupling impact on size effects of piezoresponse and conductance in mixed-type ferroelectric semiconductors.

Notably the studies [20, 21, 38-40] analyze flexoelectric and compositional effects in linear approximation, and, the most important, the appearance of domains due to spatial inhomogeneities has not been considered [see the column "Domain formation" in **Table I**]. However, one can regard that even a tiny inhomogeneity leads to the splitting of the system into domains. This result was obtained by Bratkovsky and Levanyuk [41], who performed an analytical study of stability loss and evolution of domain structure in inhomogeneous ferroelectric (or ferroelastic) samples and revealed that a tiny inhomogeneity results in the domain splitting below the phase transition temperature.

It is well-established that the spatial heterogeneity and incomplete screening of spontaneous polarization significantly influence domain structures in epitaxial thin films (see e.g. the monograph by Tagansev et al. [42] and the recent review by Roytburd et al. [43] of theoretical approaches, phase field

modeling and experimental studies of domain structures in epitaxial films). A classical results was obtained by Bratkovsky and Levanyuk [44], who studied theoretically the dielectric response of ferroelectric thin films with a "dead" dielectric layer at the interfaces with electrodes and obtained that the domain structure inevitably forms in the film in the presence of a dead layer.

While paying tribute to the previous theoretical results [20 - 40]**,** the influence of incomplete screening, combined flexo-chemical and size effects on domain structures, polar, elastic and electrophysical properties of thin ferroelectric films **have not been considered so far in a self-consistent way**. The main objective of our work is to propose a **self-consistent** approach describing the impact of the **defect driven** flexo-chemical coupling on the film properties, domain structure evolution and size effects and analyze the outcomes towards optimization of the properties for advanced applications.

Table I. Flexoelectric, Vegard and size effects, compositional gradients, and domain structure formation considered ("Yes") or no ("No") in ferroelectric thin films

References examples	**Flexoelectric, Vegard and size effects, compositional gradients, and domain structure formation considered ("Yes") or no ("No") in ferroelectric thin films**						
	Flexo-electric effect	**Compo-sition gradient, defects**	**Composi-tional polariza-tion**	**Vegard stresses**	**Flexo-chemical effect**	**Domain formation**	**Size effects**
Tilley [2]	No	No	No	No	No	No	Yes
Catalan et al [38]	Yes	Yes	No	No	No	No	Yes
Marvan et al.[23]	No	Yes	Yes	No	No	No	No
Bratkovsky, and Levanyuk [32]	No	Yes	Yes	No	No	No	Yes
Ban et al [33], Zhong et al [34]	No	Yes	No	No	No	No	No
Karthik et al. [39]	Yes	Yes	No	No	No	No	No
Morozovska et al [40]	No	Yes	No	Yes	No	Yes	No
Morozovska et al [20]	Yes	Yes	No	Yes	No	No	Yes
Morozovska et al [35],	Yes	Yes	No	Yes	No	No	Yes
Vorotiahin et al. [36]	Yes	No	No	No	No	No	Yes
Vorotiahin et al. [37]	Yes	No	No	No	No	Yes	Yes
This work	Yes	Yes	Yes	Yes	Yes	Yes	Yes

II. STATEMENT OF THE PROBLEM

The Landau-Ginzburg-Devonshire (LGD) expansion of bulk (G_V) and surface (G_S) parts of the Gibbs free energy of a ferroelectric film in powers of the polarization vector and stress tensor components P_i and σ_{ij} and the energy of the electric field outside the film (G_{ext}) have the form:

$$G = G_V + G_S + G_{ext}, \tag{1a}$$

$$G_V = \int_{V_{FE}} d^3r \left(\begin{array}{l} \frac{a_{ik}}{2} P_i P_k + \frac{a_{ijkl}}{4} P_i P_j P_k P_l + \frac{a_{ijklmn}}{6} P_i P_j P_k P_l P_m P_n + \frac{g_{ijkl}}{2} \left(\frac{\partial P_i}{\partial x_j} \frac{\partial P_k}{\partial x_l} \right) - P_i E_i \\ - \frac{\varepsilon_0 \varepsilon_b}{2} E_i E_i - \frac{s_{ijkl}}{2} \sigma_{ij} \sigma_{kl} - Q_{ijkl} \sigma_{ij} P_k P_l - F_{ijkl} \left(\sigma_{ij} \frac{\partial P_l}{\partial x_k} - P_l \frac{\partial \sigma_{ij}}{\partial x_k} \right) - W_{ij} \sigma_{ij} \delta N \end{array} \right), \quad (1b)$$

$$G_S = \int_S d^2 r \left(\frac{a_{ij}^S}{2} P_i P_j - \frac{\varepsilon_0}{2\lambda} \varphi^2 \right), \qquad G_{ext} = - \int_{\vec{r} \notin V_{FE}} d^3 r \frac{\varepsilon_0 \varepsilon_e}{2} E_i E_i . \quad (1c)$$

The tensor a_{ij} is positively defined for linear dielectrics, and explicitly depends on temperature T for ferroelectrics and paraelectrics. Below we use an isotropic approximation for the tensor coefficients $a_{ij} = \alpha_T (T - T_c) \delta_{ij}$, where δ_{ij} is the Kroneker delta symbol, T is absolute temperature, T_c is the Curie temperature. All other tensors included in the free energy (1) are supposed to be temperature independent. Tensor a_{ijklmn} should be positively defined for the thermodynamic stability in paraelectrics and ferroelectrics. Tensor g_{ijkl} determines the magnitude of the gradient energy, and is also regarded positively defined. ε_0 is the vacuum permittivity, ε_b is a relative background dielectric permittivity [45]. Coefficients Q_{ijkl} are the components of electrostriction tensor, s_{ijkl} are the components of elastic compliance tensor, F_{ijkl} is the flexoelectric strain coupling tensor. For most of the cases one can neglect the polarization relaxation and omit high order elastic strain gradient terms if the flexoelectric coefficients are below the critical values F_{ijkl}^{cr} [46, 47]. W_{ij} is the elastic dipole (or Vegard strain) tensor, that is regarded diagonal hereinafter, i.e. $W_{ij} = W \delta_{ij}$. The quantity $\delta N = N(\vec{r}) - N_e$ is the difference between the concentration of defects $N(r)$ at the point **r** and their equilibrium (average) concentration N_e .

In the surface energy Eq. (1c), the tensor a_{ij}^S and the effective surface screening length λ are introduced [37, 48]. In the isotropic approximation, $a_{ij}^S = \alpha_S \delta_{ij}$, used hereinafter, the constant α_S is related with a conventional extrapolation length Λ [2, 25], as $\Lambda = g_{11} / \alpha_S$. Concerning the physical origin of λ, we regarded that the top surface of the film is covered with the surface screening charge of the specific nature, e.g. Bardeen-type surface states [49] and so λ can be associated with a Bardeen screening length. For the case the screening charges can be localized at surface states caused by the strong band-bending via depolarization field [50, 51, 52, 53, 54], at that the value of λ can be much smaller (≤0.1 nm) than a lattice constant (~0.5 nm) [55].

Also we introduce electric field via electrostatic potential φ as $E_i = -\partial\varphi/\partial x_i$. Polarization is conjugated to the electric field E_i which can include external and depolarization contributions (if any exists).

Note that we neglected the higher elastic gradient term $\frac{1}{2}v_{ijklmn}(\partial\sigma_{ij}/\partial x_m)(\partial\sigma_{kl}/\partial x_n)$ in the functional (1b), because its magnitude and sign are still disputed [56]. Thus we apply in the following only one half ($F_{ijkl}P_k(\partial\sigma_{ij}/\partial x_l)$) of the full Lifshitz invariant $F_{ijkl}\left(P_k(\partial\sigma_{ij}/\partial x_l)-\sigma_{ij}(\partial P_k/\partial x_l)\right)/2$. The higher elastic gradient term is necessary for the stability of the thermodynamic potential if the full Lifshitz invariant is included. Application of either the term $F_{ijkl}P_k(\partial\sigma_{ij}/\partial x_l)$ or the term $F_{ijkl}\left(P_k(\partial\sigma_{ij}/\partial x_l)-\sigma_{ij}(\partial P_k/\partial x_l)\right)/2$ results in the same equations of state. The full form, however, leads to the higher order elastic equations and affects the boundary conditions [57, 58, 59, 60]. The reason of using only the part of the Lifshitz invariant in Eq. (1) is that implementation of the full form causes poor convergence of the numerical code and impairs the quality and reliability of the obtained results. Using the truncated form in Eq. (1) can be justified by the smallness of the flexoelectric coupling strength as compared to the polarization gradient term. Thus following Refs. [61, 62] we assume that the used approximation is valid if $F_{klmn}^2 << g_{ijkl}s_{ijmn}$.

Polarization distribution can be found from the Euler-Lagrange equations obtained after variation of the free energy (1)

$$a_{ik}P_k + a_{ijkl}P_jP_kP_l + a_{ijklmn}P_jP_kP_lP_mP_n - g_{ijkl}\frac{\partial^2 P_k}{\partial x_j\partial x_l} - Q_{ijkl}\sigma_{kl}P_j + F_{ijkl}\frac{\partial\sigma_{kl}}{\partial x_j} = E_i, \qquad (2a)$$

along with the boundary conditions on the top surface of the film S at $x_3 = h$:

$$\left(g_{kjim}n_k\frac{\partial P_m}{\partial x_j} + a_{ij}^S P_j - F_{jkim}\sigma_{jk}n_m\right)\Big|_{x_3=h} = 0. \qquad (2b)$$

The most evident consequences of the flexocoupling are the inhomogeneous terms in the boundary conditions (2b).

Elastic stress tensor satisfies the mechanical equilibrium equation $\partial\sigma_{ij}/\partial x_j = 0$; elastic strains are $u_{ij} = -\delta G_V/\delta\sigma_{ij}$, resulting in

$$u_{ij} = s_{ijkl}\sigma_{kl} + Q_{ijkl}P_kP_l + F_{ijkl}\frac{\partial P_l}{\partial x_k} + W_{ij}\delta N. \qquad (2c)$$

The boundary conditions at the mechanically free surface $x_3 = h$ can be obtained from the variation of the free energy (1) with respect to the stresses:

$$\sigma_{ij}n_j\big|_S = 0. \qquad (3a)$$

Here n_j are components of the external normal to the film surface. Misfit strain u_m existing at the film-substrate interface ($x_3 = 0$) leads to the boundary conditions for mechanical displacement components, U_i related to elastic strain as $u_{ij} = \left(\partial U_i / \partial x_j + \partial U_j / \partial x_i\right)/2$:

$$\left(U_1 - x_1 u_m\right)\Big|_{x_3=0} = 0, \qquad U_3\big|_{x_3=0} = 0. \tag{3b}$$

The periodic conditions were imposed at the lateral sides, $U_1\big|_{x_1=-w/2} - U_1\big|_{x_1=w/2} = wu_m$, while the period w should be defined self-consistently.

The electric field **E** (being the sum of an external $\mathbf{E}^{ext}$ and a depolarization one $\mathbf{E}^{d}$) is determined self-consistently from the electrostatic problem for the electric potential φ,

$$\varepsilon_0 \varepsilon_b \frac{\partial^2 \varphi}{\partial x_i \partial x_i} = -\frac{\partial P_j}{\partial x_j}, \tag{4}$$

supplemented by the condition of potential continuity at the top surface of the film, $z = h$, using hereinafter also notations $x_1 \equiv x, x_2 \equiv y, x_3 \equiv z$. The difference of electric displacement components $D_n^{(i)} - D_n^{(e)}$ is conditioned by the surface screening produced by the ambient free charges at the film surface *S*:

$$\left(\varphi^{(e)} - \varphi^{(i)}\right)\Big|_{x_3=h} = 0, \qquad \left(D_n^{(e)} - D_n^{(i)} + \varepsilon_0 \frac{\varphi}{\lambda}\right)\Bigg|_{x_3=h} = 0 \tag{5}$$

Here **n** is the outer normal to the film surface, electric displacement $\mathbf{D} = \varepsilon_0 \varepsilon_b \mathbf{E} + \mathbf{P}$, the subscript "*i*" means the physical quantity inside the film, "*e*" – outside the film. The conditions of zero potentials were imposed at the bottom electrode ($z = 0$) and a remote top electrode ($z = H + h$, $H \to \infty$), respectively [63] (see **Fig. 1)**.

Note, that in the case of almost homogeneous polarization (or distributed along z-axis only) the internal electric field calculated on the basis of Eqs.(4)-(5) could be easily reduced to the well-known expressions, containing the difference of the polarization and its average, $-\left(P_3 - \overline{P_3}\right)$ (see e.g. Refs.[25, 64, 65]). However, in the case of pronounced domain structure the average polarization is zero and the internal electric field is usually localized in space, in contrast to the suppositions of some approximate models, used earlier (see e.g. Refs.[26, 27]).

Note that one can associate the elastic defects in Eq. (1b) with "random temperature" defects in some sense, but we do not use this terminology, because a classical random temperature defect only renormalizes the local Curie temperature, while the elastic defects we consider are incorporated in the elastic Eq. (2c) as well as in the mechanical equilibrium equation $\partial \sigma_{ij} / \partial x_j = 0$ .Thus the Vegard stresses and strains become coupled with flexoelecricity, leading to the appearance of the term

dependent on δN in Eq. (2b) that originates from the term $F_{ijkl}\frac{\partial \sigma_{kl}}{\partial x_j}$. The defects also act as random temperature defects by renormalizing Curie temperature via electrostrictive coupling.

Further we suppose that most of defects are located in a thin top layer of thickness h_0 beyond which their concentration decreases exponentially towards the film bulk [66] (see **Fig. 1)**:

$$\delta N(z) \approx \frac{N_0}{1+\exp\left[-\left(z-h+h_0\right)/\Delta h\right]}. \qquad (6)$$

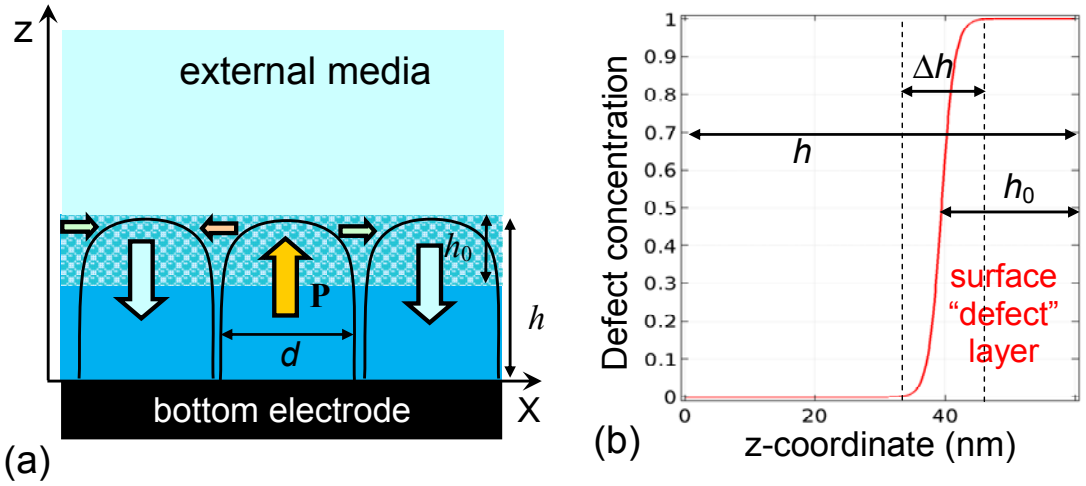

FIGURE 1. (a) Scheme of a film with the thickness h and the layer of thickness h_0 where defects are accumulated. **(b)** Normalized concentration of defects inside the layer of thickness h_0 and transition layer depth Δh. Thick arrows point the direction of polarization z-component and thin arrows point the direction of in-plane polarization components in the region of closure domains.

We suppose that the interstitial point defects with maximal concentration ~10^{26} m^{-3} [see **Table I**] can be introduced by inhomogeneous doping or implantation the PTO film with light ions, such as protons or Li, or oxygen vacancies, which may become electrically neutral inside the film due to the charge compensation by electronic carriers. It can either be "heavy" ions such as La or Bi. Also standard chemical doping may introduce neutral lattice defects like Zr substitutions on Ti sites or Ca, Cu, Co and Zn substitutions on Pb sites as first principle based calculations show [67]. A promising candidate for neutral chemical doping is Ba^{2+} substituting Pb^{2+} (see *e.g.* Ref. [68]). This substitution has larger ionic radius (135 pm against 119 pm of Pb^{2+}) and thus $W>0$. Experimentally it was proven to be possible at least in lead zirconate titanate, see Refs.[69] and [70]. All other mentioned substitutions have smaller radii than Pb^{2+} and likely provide $W<0$.In fact, the maximal molar concentration of defects in our calculations does not exceed (1 – 2)% (one defect per 50 unit cells or less), at that the volume of the cubic PTO unit cell is about 64×10^{-30} m^3. Such concentrations of doping

are quite realistic, for instance, doping with 0.5% and 1.0 mol% of Li of perovskite $Ca_xPb_{1-x}TiO_3$ was reported by Liu Jingbo et al [71]. Perovskite $SrZrO_3$ doped with 0.3 mol% of protons was studied by Slodczyk et al [72]. La doping up to 0.44mol % of $PbTiO_3$ single crystal was reported by Wójcik [73]. Piezoelectric properties of PTO ceramics doped up to 5% mol. of Bi was studied by Ueda and Ikegami [74]. The defect layer can be also formed in e.g. oxygen partial pressure condition during the film preparation, see e.g. Refs. [3, 5].

III. RESULTS AND DISCUSSION

Using COMSOL Multiphysics package © we calculated ferroelectric polarization, electric fields and elastic properties from Eqs. (2-5) for exemplarily chosen film thickness, temperature, misfit strain, the defect distribution given by Eq. (6) and $PbTiO_3$ (**PTO**) ferroelectric parameters listed in **Table II**. Results of FEM calculations are shown in **Figs. 2-7.**

Table II. Description, dimension and numerical values of material parameters

Description	**Symbol and dimension**	**Numerical value for $PbTiO_3$**
Coefficient at P^2	$\alpha(T)$ ($\times C^{-2}\cdot m$ J)	$\alpha_T(T-T_C)$
Inverse Curie-Weiss constant	α_T ($\times 10^5 C^{-2}\cdot m$ J/K)	3.8
Curie temperature	T_C (K)	752
Background permittivity	ε_b	7
Surface energy coefficient	α_{S0} ($\times C^{-2}\cdot$J)	0
Electrostriction coefficient	Q_{ij} ($\times m^4/C^2$)	Q_{11}=+0.89, Q_{12}=–0.026, Q_{44}=0.0675
Elastic stiffness tensor	c_{ij} ($\times 10^{10}$ Pa)	c_{11}=17, c_{12}=8, c_{44}=11
Elastic compliance tensor	s_{ij} ($\times 10^{-12}$ 1/Pa)	s_{11}=8, s_{12}= –2.5, s_{44}=9
Gradient coefficient	g_{ij} ($\times 10^{-10} C^{-2} m^3$ J)	g_{11}=4.0, g_{12}= –0.5, g_{44}=0.5,
Flexoelectric stress tensor	f_{ij} (V)	f_{11}=6.8, f_{12}=4.9, f_{44}=5.6
Flexoelectric strain tensor	F_{ij} ($\times 10^{-11} m^3/C$)	F_{11}=3, F_{12}=1, F_{44}=5 *
Kinetic coefficient	Γ ($\times$s m/F)	100
LGD-coefficient at P^4	a_{11} ($\times 10^8$ JC$^{-4}\cdot$m^5)	–0.73
LGD-coefficient at P^6	a_{111} ($\times 10^8$JC$^{-6}\cdot$m^9)	+2.60
Surface screening length	λ ($\times 10^{-10}$m)	1 (or vary within the range)
Vegard strain coefficient	W ($\times 10^{-30}$m)	±10 **
Misfit strain	u_m (%)	–1
Maximal defect concentration	N_0 ($\times 10^{26}$ m^{-3})	(0 – 3)
Defect layer thickness	h_0 (nm)	25
Transition layer depth	Δh (nm)	1

* The coefficients F_{ij} are still not available experimentally for PTO, but some components could be evaluated from the first principles for various perovskites [75, 76, 77] and their thin films [78]. On the other hand, the magnitudes of F_{11}= 3, F_{12}= 1 and F_{44}= 0.5 (in $10^{-11}C^{-1}m^3$ units) are of the same order as the microscopic estimations ($F\sim 10^{-11}m^3/C$) by Kogan, and the values measured for $SrTiO_3$ by Zubko et al. [79, 80]. The value $F_{44}=5\times 10^{-11}C^{-1}m^3$ is higher than a conventional one, but its effect is only relevant for fine details of polarization

and elastic field distributions close to the bottom electrode. We note also that all values we used are significantly smaller than the ones [F~(5-10)$\times 10^{-10}$m^3/C] measured for $PbZrTiO_3$ by Ma and Cross [81].

** The chosen values of Vegard coefficient, W=±10A are in agreement with ab initio calculations for perovskite SrTiO3 [14] as well as with typical experimental values [16-17].

A. Polarization, domain structure and elastic field dependence on the sign of Vegard coefficient

Note, that in most cases, a stable poly-domain structure with prevailing out-of-plane polarization has been found for an applied negative misfit strain u_m = -1% and λ>0.1nm [37], which support the out-of-plane polarization component [8] and a poly-domain structures. The appearance of the closure domains [42] under the electrically open film surface depends strongly on the degree of screening, represented by the values of the surface screening length λ and temperature [37].

To illustrate the above mentioned issues, **Fig. 2** shows the spatial distributions of the in-plane and out-of-plane polarization components, P_x and P_z, respectively, corresponding elastic strains u_{xx} and u_{zz}**,** and von Mises stress [82],

$$\sigma_v = \sqrt{\left(\sigma_{xx}-\sigma_{yy}\right)^2+\left(\sigma_{yy}-\sigma_{zz}\right)^2+\left(\sigma_{zz}-\sigma_{xx}\right)^2+6\sigma_{yz}^2+6\sigma_{zx}^2+6\sigma_{xy}^2}\,, \qquad (7)$$

in the cross-section of a 50-nm thick PTO film. The top and bottom rows are calculated for positive and negative Vegard coefficients, $W=+10\,\text{Å}$ and $W=-10\,\text{Å}$, respectively. At elevated temperature T=600 K, which, however, is sufficiently far from the film's transition temperature to the paraelectric phase, shallow (up to 5 nm) closure *a*-domains appear near the electrically open surface. They have a form of rounded wedges and relatively diffuse domain walls [see **Fig. 2(a)** and **2(f)** showing P_x distribution]. There are clearly visible stripe *c*-domains with relatively sharp domain walls in the middle of the film and near the bottom screening electrode for the normal component of the polarization. The stripe domain walls noticeably broaden and diffuse to the depth of about 5 nm near the top surface [see **Fig. 2(b)** and **2(g)** showing P_z distribution]. The polarization in the middle of the closure and stripe domains is significantly larger for the Vegard coefficient $W=+10\,\text{Å}$, than it is for $W=-10\,\text{Å}$, but all other characteristics of *a*- and *c*- domains depend weakly on the value of W [compare **Fig. 2(a)** and **2(f), Fig. 2(b)** and **2(g)**]. A 25 nm layer of elastic defects, the domain structure, and the misfit strain at the film-substrate interface determine the structure and spatial distribution of the elastic strain tensor in the film, whose diagonal components u_{xx} and u_{zz} are shown in **Fig. 2(c), 2(d)** and **2(h), 2(i)**, respectively**.** The main features on the lateral strain distribution are caused by the domain structure via the piezoelectric and flexoelectric effects, and so the distribution of u_{xx} is virtually independent on the sign of W [compare **Fig. 2(c)** and **2(h)**]**.** The main features of the vertical strain distribution are conditioned not only by the domain structure, but also by an elastic field gradient in the

defect layer. That is why a diffuse horizontal boundary is clearly visible on the edge of the defect layer in **Fig. 2(d)** and **2(i)**. The vertical strain in this layer is determined by a chemical pressure of defects and thus it changes sign when the sign of W is changed [compare **Fig. 2(d)** and **2(i)**]. The distribution of von Mises dilatational stress σ reproduces the profile of the out-of-plane polarization component, namely, a stripe domain structure with broadened domain walls near the surface while the value of σ, in a near-surface layer with a thickness of the order of 5 nm, is strongly dependent on the sign of W [see **Fig. 2(e)** and **2(j)**]. We note that the pronounced features of the distributions of u_{xx}, u_{zz} and σ near the bottom electrode do not depend on the sign of W, since they arise from the flexoelectric coupling.

Note that the value of the screening length λ strongly affects the polar properties of the film, determines its critical thickness at fixed temperature and the existence as well as the type of the domain structure [37]. In addition, a pronounced minimum at a certain width, which depends on W, temperature and film thickness, appears on the dependence of the system specific energy E on the domain lateral size d when λ increases [see **Fig.3**]. The decreasing dependence $E(d)$ is steeper, and the minimum on it is much deeper for positive $W = +10\,\text{Å}$ than for negative $W = -10\,\text{Å}$ [compare **Figs. 3(a)** and **3(b)**].

Notably, the expected Kittel-Mitsui-Furuichi (**KMF**) relation connecting the period d of the stripe domain structure having infinitely thin walls with the film thickness h, $d \sim \sqrt{h}$, is not confirmed in our calculations, since they naturally account for domain wall broadening near electrically-open surfaces (via the polarization gradient [83]) and closure domains (via polarization rotation) [40]. Moreover, our results are λ- and W-dependent. To illustrate this, **Fig. 3(c)** shows the dependences of the equilibrium domain size d on the screening length λ. The dependence on the domain size on λ obeys an analytical formula, $d = d_0 + \dfrac{D}{\lambda - \lambda_{cr}}$ [see **Fig. 3(d)** showing the dependence of inverse value $1/(d - d_0)$ on λ]**,** where the critical values λ_{cr} slightly differ for $W = +10\,\text{Å}$ and $W = -10\,\text{Å}$, while the parameters d_0 and D depend on the W sign much more strongly [see caption to **Fig. 3**].

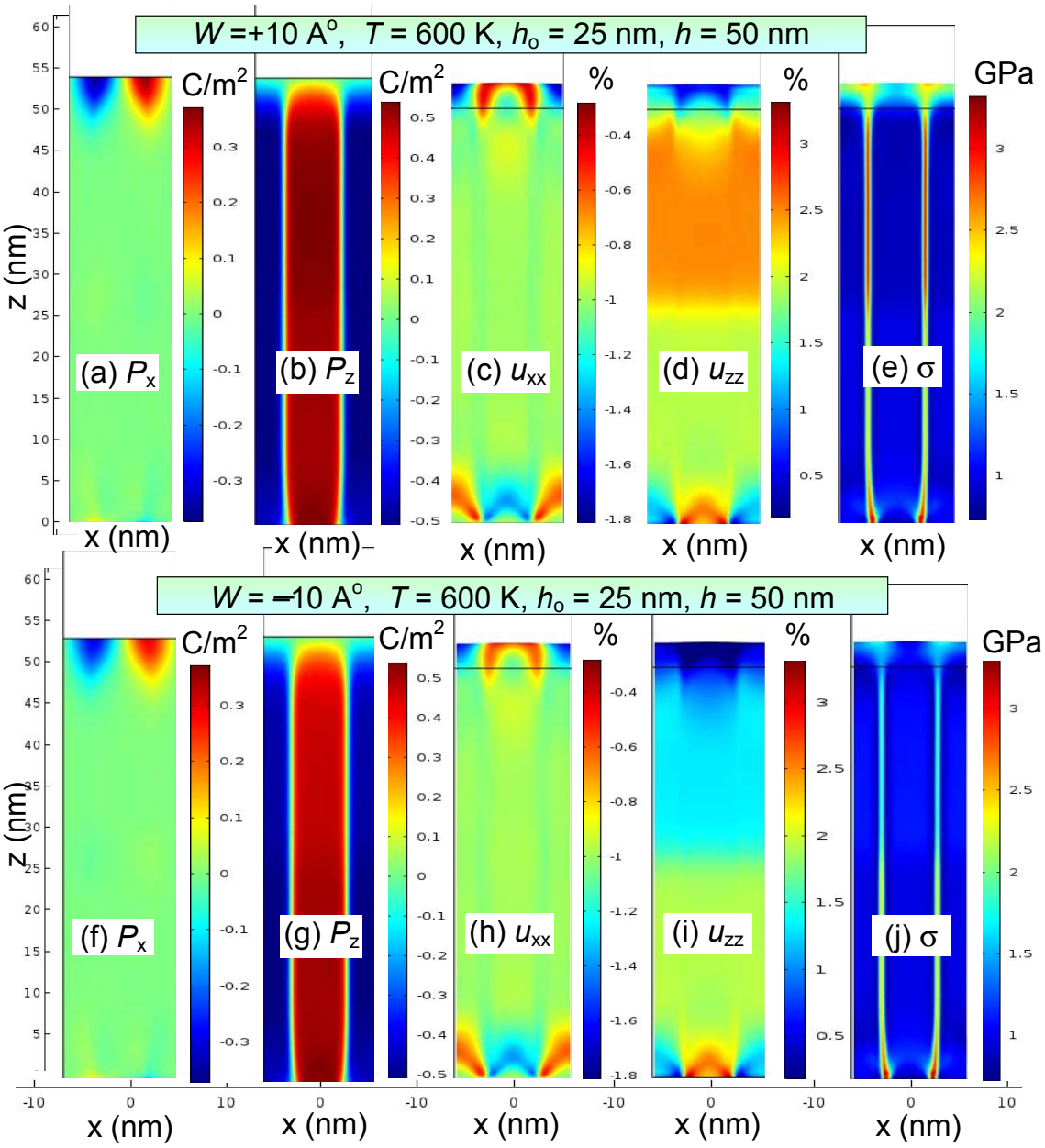

FIGURE 2. Spatial distribution of the in-plane polarization component P_x **(a,f)** and the out-of-plane component P_z **(b,g)**, elastic strains u_{xx} **(c,h)** and u_{zz} **(d,i),** and von Mises stress σ **(e,j)** in the cross-section of the 50-nm PTO film calculated for positive [top row, plots **(a-e)**] and negative [bottom row, plots **(f-j)**] Vegard coefficients $W = \pm 10\,\text{Å}^{\circ}$, temperature T=600 K, screening length λ=0.1nm, depth of defect layer h_0=25 nm, Δh=1 nm, and defect concentration $N_0 = 3\times10^{26}$ m^{-3}. Other parameters are listed in **Table II.**

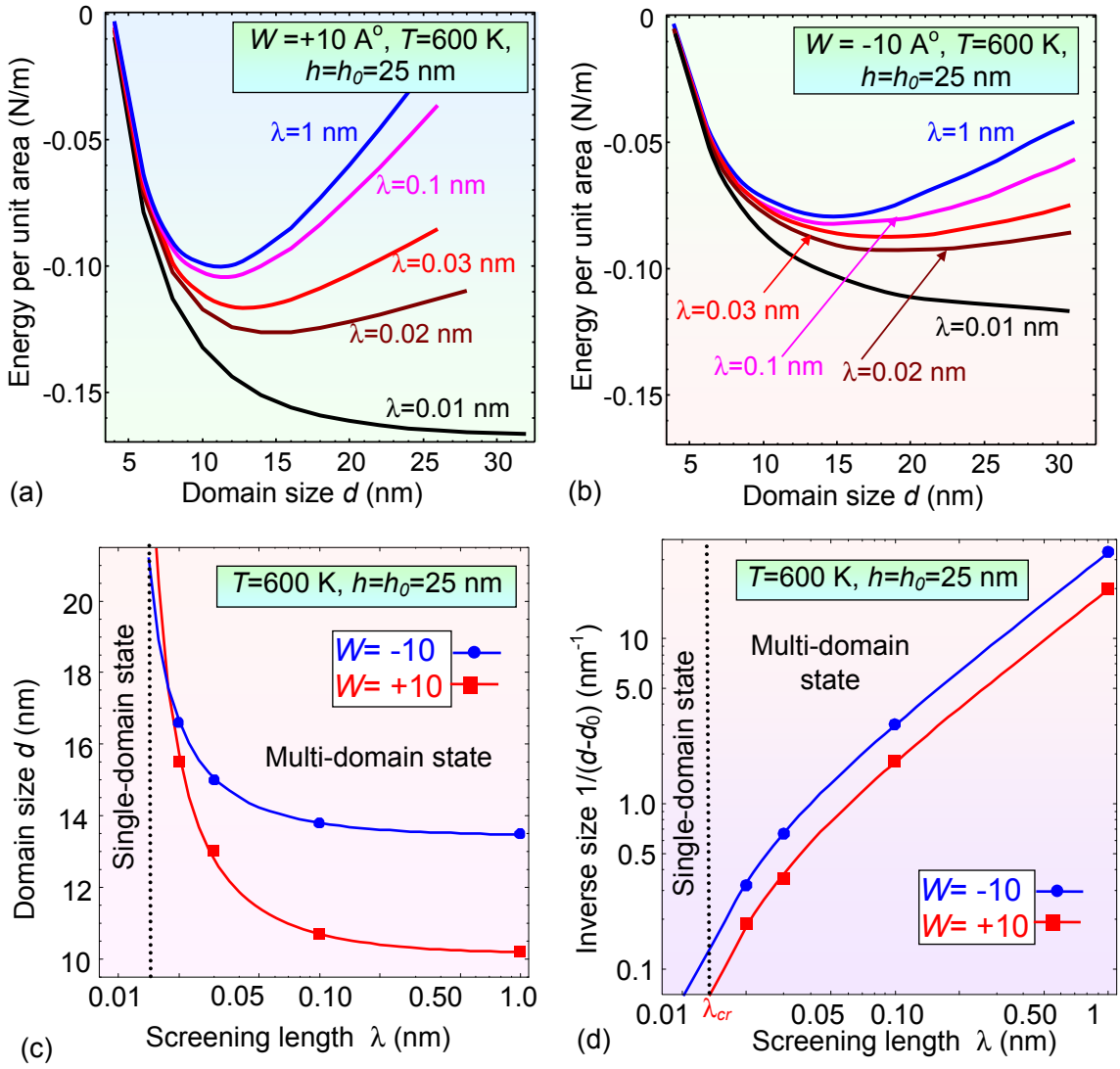

FIGURE 3. (a) The dependence of the 25-nm thick $PbTiO_3$ film total energy on the domain size (potential relief of wall-wall interaction) calculated for different values of surface screening length λ (shown near the curves), positive Vegard coefficient $W = +10\,\text{Å}$ **(a)** and negative Vegard coefficient $W = -10\,\text{Å}$ **(b)**. Dependences of the equilibrium domain size d **(c)** and inverse value $1/(d - d_0)$ **(d)** on the surface screening length λ calculated numerically for $W = -10\,\text{Å}$ (circles) and $W = +10\,\text{Å}$ (squares). Solid curves are fitting to the formula $d = d_0 + \dfrac{D}{\lambda - \lambda_{cr}}$, where $d_0 = 13.5$ nm, $D = 0.03$ nm^2, $\lambda_{cr} = 0.010$ nm for $W = -10\,\text{Å}$; and $d_0 = 10.2$ nm, $D = 0.05$ nm^2 and $\lambda_{cr} = 0.011$ nm for $W = +10\,\text{Å}$. Temperature T=600 K and defect concentration $N_0 = 3\times10^{26}$ m^{-3}. Other parameters are listed in **Table II.**

Notably the limit of "ideal metal" corresponds to $\lambda = 0$, while it was shown earlier that there is a finite non-zero value of λ below which the polydomain film transforms into monodomain state (see

e.g. Ref.[84] for uniaxial ferroelectric, when closure domains are absent, and Ref. [37] for multiaxial ferroelectrics).

B. Temperature evolution of spontaneous polarization, domain structure and elastic fields

Figure 4 shows the temperature dependencies of the maximum spontaneous polarization P_S at the center of the stripe domains, calculated for films of different thicknesses (6 – 50) nm with a layer of elastic defects (solid curves) and without it (dashed curves). Note that the presence of defects noticeably enhances the value of switchable polarization $2P_S$ (dashed curves are always lower than solid ones) in PTO films with thickness less than 50 nm, but due to the stripe domain structure the average polarization is zero without applied electric field. Due to defects, corresponding switchable bound charge $\sigma_S = 2P_S$ increases significantly [up to (40-80)μC/cm^2] in the vicinity of phase transition temperature that varies in the range (750 – 950)K depending on the film thickness [compare the onset of solid and dashed curves in **Fig. 4(a)**]. At room temperature the increase of σ_S induced by defects is much smaller (~5 μC/cm^2).

Moreover, the temperature of the spontaneous polarization and domain structure appearance in a film with defects is much larger (by 50 – 70 K), than for films without them, and the polarization itself is somewhat larger for thin films with a thickness less than 25 nm, for which the defect layer occupies the whole film and the Vegard effect is positive ($W = +10\,\text{Å}$) [compare solid and dashed curves in **Fig. 4(a)**]. When increasing the film thickness to 50 nm (with a thickness of the defect layer 25 nm), the temperature of the spontaneous polarization emergence becomes 20 K higher than the ferroelectric transition temperature of a 50-nm film without defects [compare solid and dashed curves in **Fig. 4(b)**]. Notably, the bending appears on the temperature dependence of the maximum polarization at the temperature 550 K, being related with the emergence of closure domains at lower temperatures. The temperature of polarization emergence decreases at negative $W = -10\,\text{Å}$ (this case is not shown in the figures, since we are primarily interested in the conditions of polar properties enhancement).

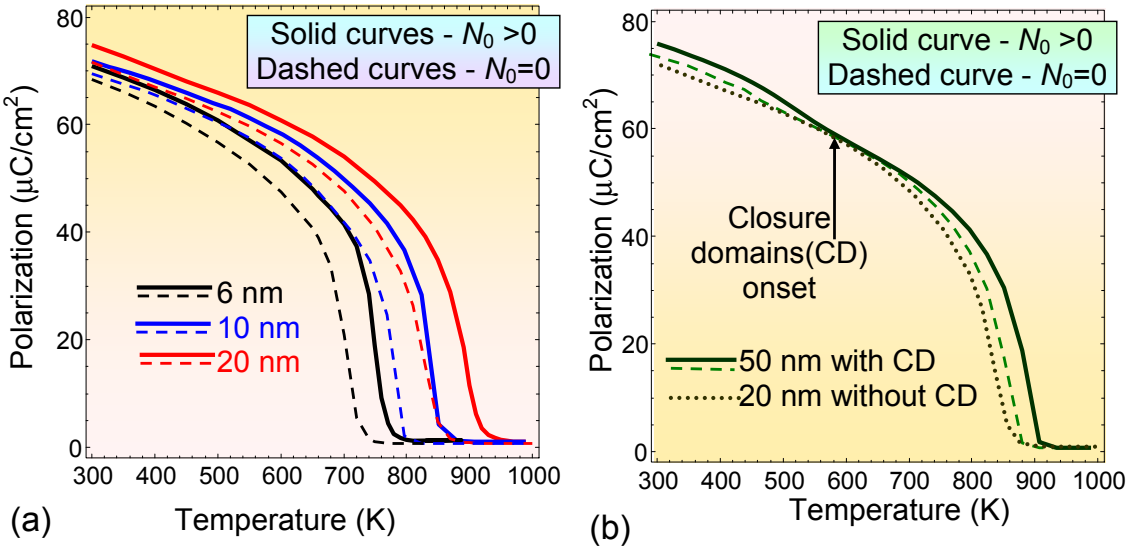

FIGURE 4. Temperature dependence of the maximal spontaneous polarization calculated for different film thicknesses h = (6, 10, 20) nm [plot **(a)**] and h = (20, 50) nm [plot **(b)**], without defects ($N_0 = 0$, dashed curves) and with defect concentration $N_0 = 2\times10^{26}$ m^{-3} and Vegard coefficient $W = +10$ Å [plot **(b)**], screening length λ=0.1nm. Other parameters are listed in **Table II.** The inflections at the curves for 50-nm thick film indicate the appearance of the closure domains (CD) at temperatures lower than 550 K.

Spatial distributions of in-plane and out-of-plane polarization components and corresponding elastic strains in the cross-section of the 60-nm thick PTO film calculated for positive Vegard coefficients $W = +10$ Å, elevated (850 K) and room (300 K) temperatures are shown in **Fig.5.** It is evident that the closure domains, as well as a pronounced stripe domain structure, are absent at high temperatures near the phase transition of the film into the paraelectric phase [compare **Figs. 5(a)-(d)** and **5(e)-(h)**]. On the contrary, small domains, which branch near the surface of the film, appear at 850 K. They gradually "freeze" and transform to stripe domain structure with closure domains as the temperature decreases.

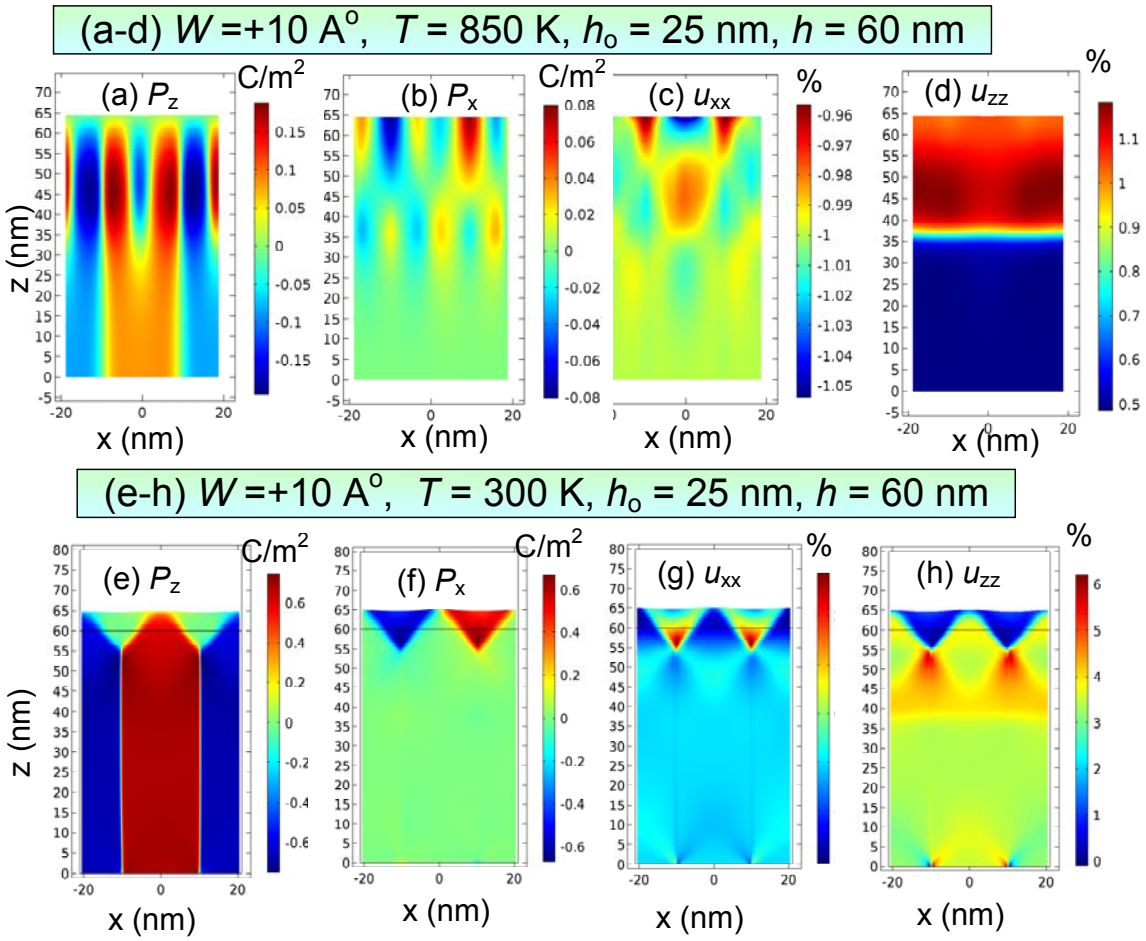

FIGURE 5. Spatial distributions of polarization components P_z **(a, e)** and P_x **(b, f)**, elastic strains u_{xx} **(c, g)** and u_{zz} **(d, h)** in the cross-section of the 60-nm thick PTO film calculated for positive Vegard coefficients $W = +10\,\text{Å}$, temperatures T=850 K [plots **(a)-(d)**] and 300 K [plots **(e)-(h)**], screening length λ=0.1nm and defect concentration $N_0 = 3\times10^{26}$ m^{-3}. Other parameters are listed in **Table II.**

C. Ferroelectric transition temperature dependence on the film thickness

Figure 6 shows the dependence of the ferroelectric transition temperature $T_C(h)$ on the film thickness h [**Fig. 6(a)**] and its inverse value $1/h$ [**Fig. 6(b)**], calculated for the positive, zero and negative Vegard coefficients W. At $W > 0$ the maximum appears on the dependence at a film thickness of 25 nm, virtually equal to the thickness of the defect layer h_0 [see red curve in **Fig. 6(a)**]. Temperature $T_C(h)$ decreases monotonically with decreasing h at $W \le 0$. Notably, the inequality $T_C(h, W<0) < T_C(h, W=0) < T_C(h, W>0)$ is valid for thicknesses more than 4 nm [compare red, magenta and blue curves in **Fig. 6(a)**]. At a film thickness of about 3.5 nm, all three curves intersect, and the order of the curves corresponding to $W > 0$ and $W < 0$ changes with the further decrease of

the film thickness. A maximum and a kink on dependencies $T_C(h)$ are observed at $h = h_0$, for positive and negative *W*, respectively [see red and blue curves in **Fig.6(a)**].

From **Figure 6(a)** we can see, that the critical thickness of the film below which the ferroelectric phase vanishes is absent for all *W*. It is true even until 2 nm thickness (that is about 5 lattice constants) for which the continual theory of LGD is still applicable at least qualitatively. Somewhat overstretching the LGD approach one can observe in **Figure 6(b)** that T_C does not decrease below room temperature for the films with thickness $h \geq 1$ nm or even less, its value varying within the range (350-450) K in dependence on the sign and value of *W* [compare red, magenta and blue curves with symbols in **Figs. 6**]. This effect can be explained only by the presence of relatively strong compressive strains (-1%) at the film-substrate interface, which effectively support spontaneous dipole displacements in ulta-thin films [3-5] due to the electrostriction [8] and flexoelectric effect [40]. The depolarization field in the film is minimal due to a developed domain structure [see **Figs. 2** and **4**]. Indeed, electrostrictive coupling between polarization and elastic stresses shifts the transition temperature significantly, in the order of $Q_{33ij}\sigma_{ij}/\alpha_T$ in a stressed film (see ref. [8] for details), and the flexoelectric effect creates a built-in electric field proportional to the convolution of tensors $F_{jkim}\sigma_{jk}n_m$ in the boundary conditions Eq. (2b) (see ref.[40] for details). The approximate part of the dependence $T_C(h)$ calculated analytically for small thicknesses without the flexoelectric effect and Vegard effect is shown in **Fig. 6 (b)** by a dotted curve.

Room temperature spontaneous polarization P_S in dependence on the film thickness is shown in **Fig. 6(c).** Since one can regard that $P_S(h) \sim \sqrt{T_C(h) - T}$ within LGD-approach, the value P_S becomes almost thickness-independent or even slightly increasing with thickness decrease below 2 nm for nonzero flexocoupling [see red, magenta and blue curves with symbols in **Fig. 6(c)**]. Corresponding switchable bound charge σ_S is equal to $2P_S$.

Without flexocoupling and defects the spontaneous polarization sharply disappears with thickness decrease and the size-induced transition into a paraelectric phase occurs at *h*=3 nm [see dotted curve in **Fig. 6(c)**]. At that the difference between the switchable polarization calculated for nonzero flexocoupling at positive and negative Vegard coefficients is about 12 μC/cm^2, leading to the difference of about 24 μC/cm^2 in the switchable bound charge. Hence we can predict that the relatively high switchable polarization of order (50 - 60) μC/cm^2 and switchable bound charge σ_S about (100 - 120) μC/cm^2 can be induced in ultrathin PTO films due to the flexo-chemical effect. The predicted increase of $\sigma_S \sim (0.2 - 1)$ C/m^2 in ultrathin perovskite films of thickness less than 5 nm is due to the flexo-chemical effect; and it can be important for applications in advanced memory devices opening the way for their further miniaturization.

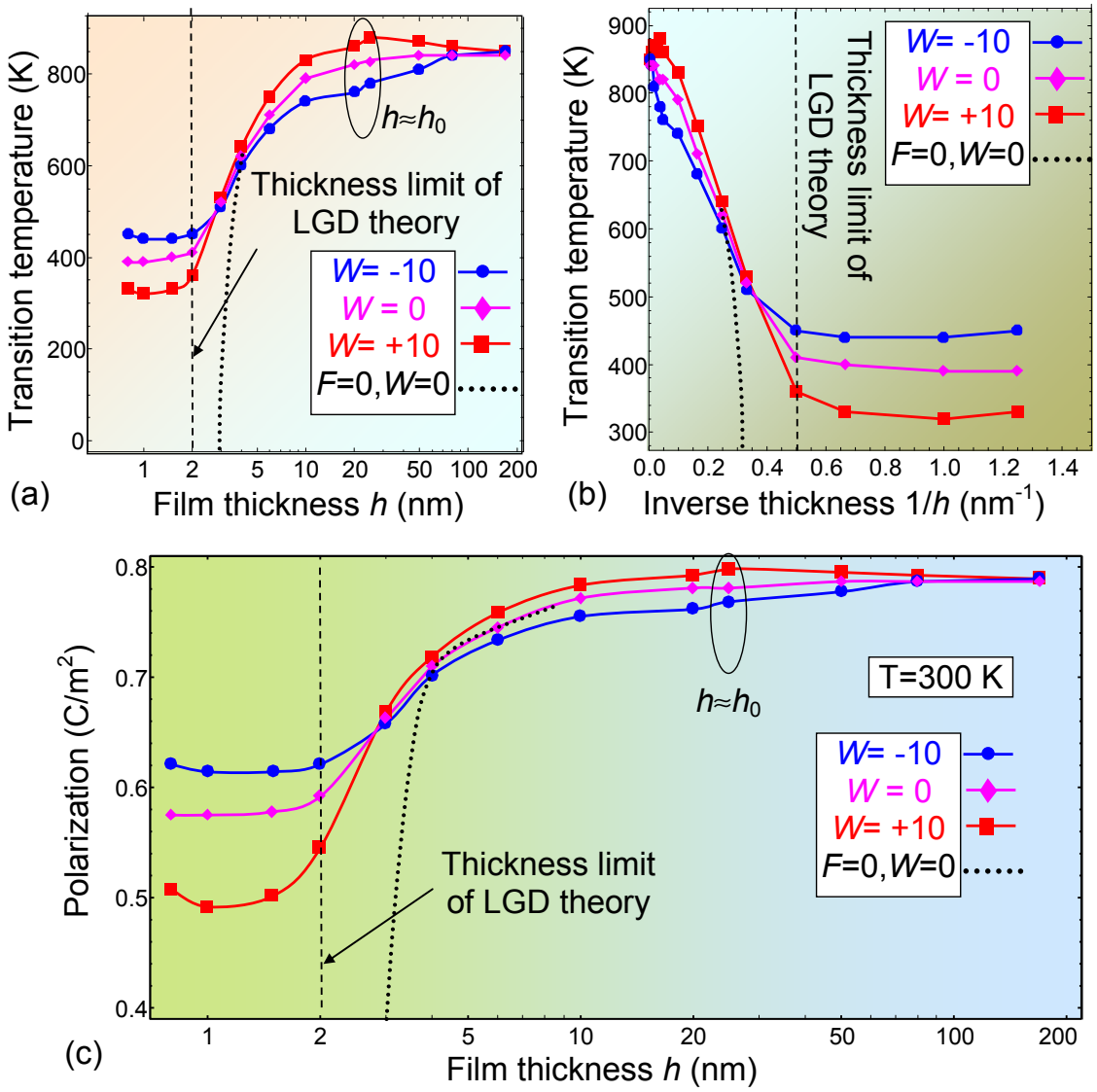

FIGURE 6. Ferroelectric transition temperature vs. the film thickness h **(a)** and $1/h$ **(b)**. The spontaneous polarization in dependence on the film thickness calculated at T=300 K **(c).** Screening length λ=0.1nm, $N_0 = 3\times10^{26}$ m^{-3}, Vegard coefficient $W = +10$ Å (squares), $W = 0$ (diamonds) and $W = -10$ Å (circles), and nonzero flexocoupling. Dotted line in plots **(b,c)** correspond to the simultaneous absence of the flexoelectric coupling and Vegard effect, $W = 0, F = 0$. Vertical dashed lines indicate the thickness limit of continuum LGD-theory applicability. Other parameters are listed in **Table II.**

Distributions for the 2-nm film calculated at the temperature 300 K show the film in the state close to the phase transition; that is why its polarization is severely weakened and domain walls are notably diffused. Also, a metastable domain state can be observed for the film at negative W. This illustrates sensitivity of thin films to lateral boundary conditions and flexoeffect that carry a major

responsibility for the formation of such kinds of structures. Flexoelectric coupling, in particular, is also responsible for the very existence of the ferroelectric phase in thin films under 6 nm.

A possible explanation for an anomalous change in the phase-transition curve evolution at h<4 nm [that is shown in **Fig. 6(a)**] could be a transition from the c-domain state of the film with polarization perpendicular to the surface in thick films (where a part of closure domains is relatively small because of their localization at approximately 5 nm below the surface, see **Figs. 2** and **5**) to the mainly a-domain state with the decrease of thickness, owing to the flexocoupling. Indeed, with the thickness decrease a-domains with the in-plane polarization direction become significant (see **Fig. 7**). This happens because it is well known that compressive misfit strains u_m<0 support the c-domain formation, while the dilatation ones u_m>0 support the a-domain formation. Respectively, W>0 supports c-domain stability, while W<0 supports the stability of a-domains. Therefore, for the case of thickness decrease below 4 nm in the film already having defects homogeneously occupying its whole bulk (because h_0=25 nm >> 4 nm), it is energetically favorable to increase the fraction of a-domains, so that the ferroelectric phase transition temperature for this scenario is higher. This can be seen in **Fig. 6**; the detailed analysis of the corresponding domain structure and elastic fields for the film thicknesses below 5 nm is given in **Fig. 7**.

Polarization components change their behavior when the film thickness approaches 4 nm and less. The out-of-plane component that prevailed in thicker films gradually dims, giving the place for the in-plane polarization rising amplitude and growing area of closure domains. 3-nm film is already seen as such where the a-domains slightly exceed the c-domains in size. While the sign of the Vegard effect coefficient has an insignificant effect on the polarization amplitude and domain shapes, it can change mechanical strain and stress distributions. It can be seen in **Fig. 7** that there are different elastic fields, specifically the out-of-plane component u_{zz}, changing significantly under positive and negative W, which can be consistently traced back to the thicker films (see **Fig. 2**), where such dependencies occur in the defect-rich part of a ferroelectric bulk. Since defects are quasi-uniformly spread across the depth of the thin film (h_0 >> h), Vegard stresses impact the whole film thickness. Note that the asymmetry of the out-of-plane polarization scale (from –0.45 to 0.6 C/m²) at film thickness 2-3 nm originates from the built-in electric field induced by flexo-chemical coupling, and the asymmetry is absent for thicker films [compare **Figs.7** with **Figs. 2** and **5**]. Temperature dependence of the total energy per unit area in the films of thickness (2 – 170) nm is shown in Appendix A.

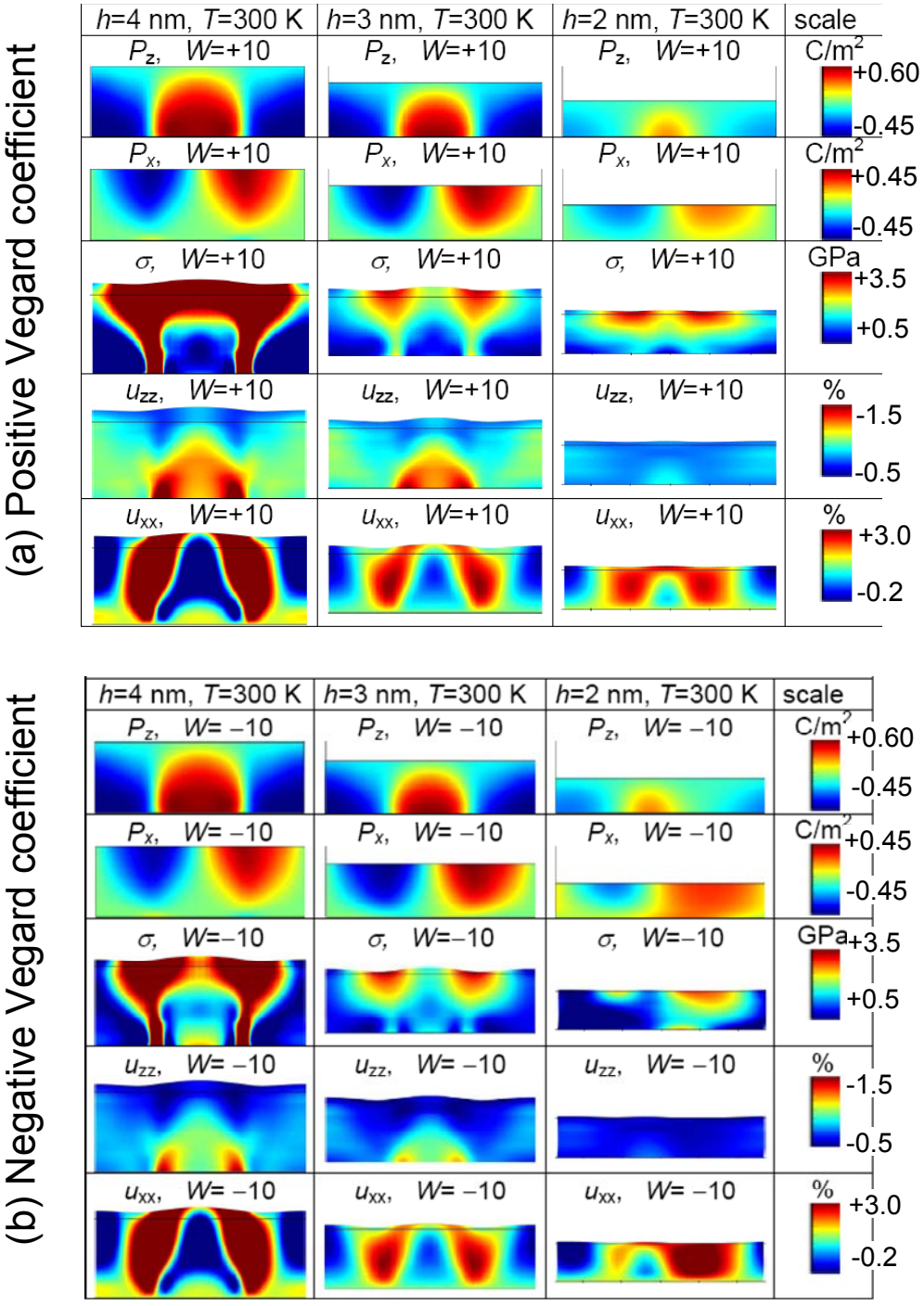

FIGURE 7. Spatial distribution of the out-of-plane and in-plane polarization components P_x and P_z, von Mises stress σ and elastic strains u_{xx} and u_{zz} in the cross-sections of the 4, 3 and 2-nm PTO film calculated for positive [top part **(a),** $W = +10\,\text{Å}$] and negative [bottom part **(b),** $W = -10\,\text{Å}$] Vegard coefficients, room temperature T=300 K, screening length λ=0.1nm, and defects filling the entire film with a concentration $N_0 = 3\times10^{26}$ m^{-3}. Other parameters are listed in **Table II.** Color gradient denotes scales of for the following physical parameters. In-plane polarization changes from –0.45 to 0.45 C/m²; out-of-plane polarization changes from –0.45 to 0.6

C/m²; Von Mises stress changes from 0.8 to 3.6 GPa; in-plane strain changes from −1.7% to −0.3%; out-of-plane strain changes from –0.2% to 3.1%.

Graphs in **Figs. 6-7** are plotted for the fixed concentration of defects. Their detailed analysis, carried out for various defect concentrations in the temperature range of (600 – 900) K with a positive Vegard coefficient, shows, that a pronounced maximum appears on the transition temperature dependence $T_C(h)$ at $h \approx h_0$ with the increase of the defect concentration [see **Fig. 8(a)** in a semi-logarithmic graph]. At the maximum, the transition temperature of (20-30) nm film with a layer of defects near the surface exceeds by 50 K the transition temperature of a thick lead titanate film, which makes it possible to significantly improve the polar properties of thin films. The transition temperature of (20-30) nm film without defects is about 200 K lower than the one in the film with defect concentration 3×10^{26} m^{-3} and $W = +10\,\text{Å}$. Note that we neglected the relaxation of the mismatch deformations in films with thickness $h > h_0$, and therefore the applied compressive strain (-1%) leads to renormalization of the Curie bulk temperature from 752 K to 880 K in 100-nm films.

Dependence of transition temperature on the defect concentration N_0 increases quasi-linearly at $W > 0$, and its slope increases with the film thickness decrease [**Fig. 8(b)**]. Solid curves with empty symbols in **Fig. 8(a)** and dashed curves in **Fig. 8(b)** calculated accounting for the flexoelectric effect with flexoelectric coefficient $F_{ij} > 0$ listed in **Table I** correspond to a higher $T_C(h)$ than the curves calculated at $F_{ij} = 0$. The difference is most significant for the thinnest films [see the curves for *h*=10 nm and 20 nm in **Fig. 8(b)**]; it decreases with the film thickness increase and is almost nondescript for the films with a thickness in the order of 100 nm and above [see the curves for *h*=80 nm and 170 nm in **Fig. 8(b)**]. This is obviously related with the built-in electric field induced by the flexoelectric coupling of polarization with inhomogeneous elastic stresses, which is proportional to the product $F_{jkim}\sigma_{jk}n_m$ [see boundary conditions (2b)]. Note that the transition temperature substantially rises with defect concentration increase at positive Vegard coefficient (with the flexoeffect or without it), but the reentrant ferroelectric phase, observed experimentally in spherical nanoparticles with a radius $R < 5$ nm [22] and then explained theoretically by flexo-chemical coupling [21], has not been observed in thin films. In our opinion this is because there is no curved surface in the films that induces the ferroelectric phase due to a competition between the contributions of size effects and surface tension into the Curie temperature shift, which have different signs and are proportional to $1/R$ and $1/R^2$, respectively [21].

Room temperature spontaneous polarization P_S in dependence on the film thickness is shown in **Fig. 8(c)** for various defect concentrations N_0 within the range $(0 - 3)10^{26}$ m^{-3} and positive Vegard

coefficient $W = +10\,\text{Å}$. Without defects P_S monotonically increases with the film thickness increase. Since $P_S(h) \sim \sqrt{T_C(h) - T}$ the polarization curves have maxima at $h \approx h_0$ with the increase of the defect concentration over about 10^{26} m^{-3} [see red, magenta and blue curves with symbols in **Fig. 8(c)**]. However a corresponding difference (0.03 C/m^2) of the maximal value 0.81 C/m^2 at $N_0 = 3\times10^{26}$ m^{-3} in comparison with 0.79 C/m^2 at $N_0 = 0$ is much smaller than the difference between the corresponding curves (~0.79 C/m^2) for thin films [compare red, magenta and blue curves in **Fig. 8(c)** with the corresponding ones in **Fig. 6(c)**].

Dependence of the spontaneous polarization on defect concentration N_0 calculated at 300 K for different film thicknesses (~10 – 200 nm) is shown in **Fig. 8(d)**. Polarization is increasing gradually with N_0 increase at positive Vegard coefficient, at that the slope essentially increases with the film thicknesses decrease [compare black, red, green, magenta and blue curves in **Fig. 8(d)**]. Also the difference between the curves calculated with and without flexoelectric coupling increases strongly with the film thickness decrease [compare solid and dashed curves in **Fig. 8(d)**]. In particular the spontaneous polarization of 10 nm film substantially rises (from 0.35 C/m^2 to 0.45 C/m^2) with defect concentration increase from 0 to 3×10^{26} m^{-3}. At that the polarization curve calculated allowing for the flexocoupling in a 10-nm film is essentially higher (~0.1 C/m^2) than the one calculated without it [compare solid and dashed black curves in **Fig. 8(d)**]. Corresponding switchable bound charge σ_S is approximately equal to 0.7 C/m^2 at $N_0 = 0$ and $F_{ij} = 0$, and can reach the value 0.98 C/m^2 at $F_{ij} > 0$ and $N_0 = 3\times10^{26}$ m^{-3}. The predicted increase of the switchable bound charge ~0.28 C/m^2 due to the flexo-chemical effect can be important for thin films applications in memory devices.

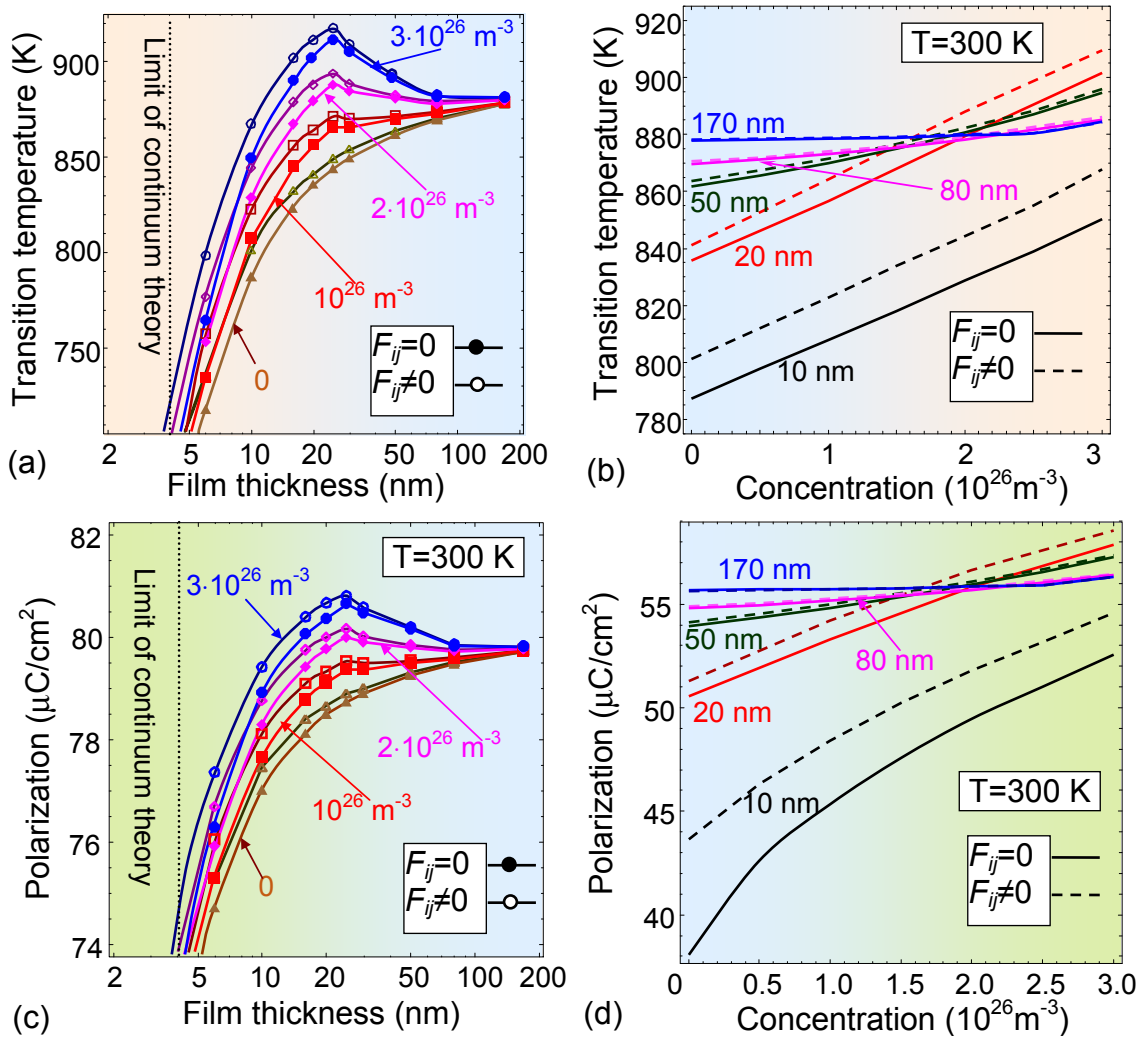

FIGURE 8. Ferroelectric transition temperature dependence on the film thickness and defect concentration. **(a)** Dependence of the transition temperature on the film thickness calculated for different values of the defect concentration N_0 (shown near the curves) and zero (empty symbols) or nonzero (filled symbols) flexoelectric coefficients. **(b)** Dependence of the transition temperature on defect concentration calculated at 300 K for different values of the film thickness (shown near the curves) and zero (solid curves) or nonzero (dashed curves) flexoelectric coefficients. **(c)** Dependence of the spontaneous polarization on the film thickness calculated at T=300 K and different values of the defect concentration N_0 (shown near the curves) and for zero (empty symbols) or nonzero (filled symbols) flexoelectric coefficients. **(d)** Dependence of the spontaneous polarization on defect concentration calculated at 300 K for different values of the film thickness (shown near the curves) and zero (solid curves) or nonzero (dashed curves) flexoelectric coefficients. Screening length λ=0.1nm, $W = +10\,\text{Å}$, and the depth of the defect layer h_0=25 nm, Δh=1 nm,. Other parameters are listed in **Table II.**

The pronounced maximum on the transition temperature contour maps in the variables "film thickness - defect concentration" exists under the presence of flexoelectric coupling [see **Fig. 9(a)**] and

without it [see **Fig. 9(b)**], however, the flexoelectric effect significantly shifts the transition temperature (by up to 30 K for thin $PbTiO_3$ films).

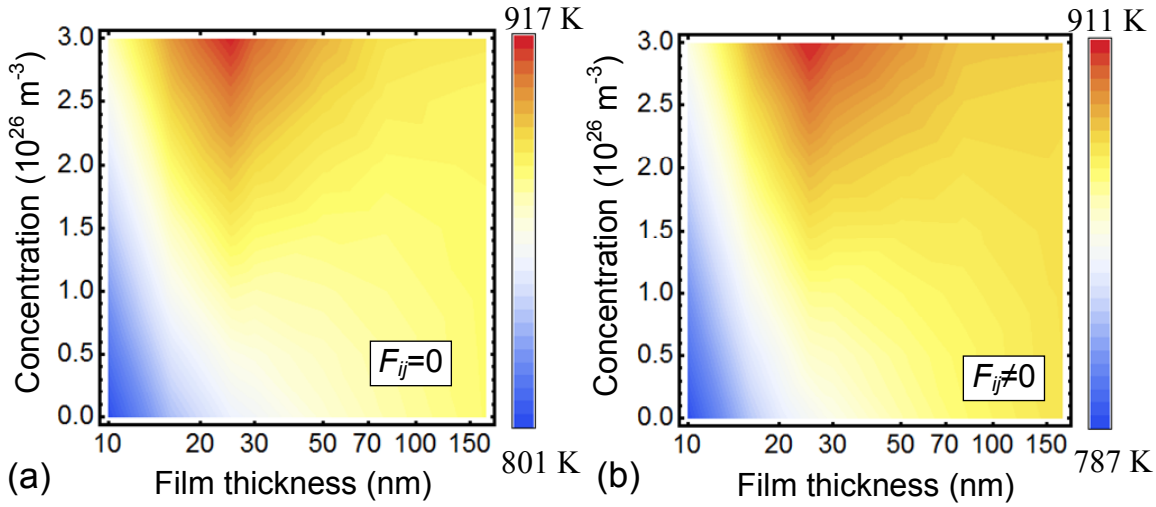

FIGURE 9. Contour maps in the coordinates "film thickness – defect concentration" for the two cases of zero **(a)** and nonzero **(b)** flexoelectric coefficients. Room temperature, screening length λ=0.1nm, $W = +10\,\text{Å}$, and the depth of defect layer h_0=25 nm, Δh=1 nm,. Other parameters are listed in **Table II.**

Thus, the position and height of the maximum $T_C(h)$ can be controlled by the defect concentration in the layer and the surface screening length, which can be useful for advanced applications. Summarizing this section, we conclude that uncharged elastic defects have an unexpectedly strong impact on the polar and elastic properties of ferroelectric films due to Vegard stresses in the defective layer of the film and the flexoelectric effect.

Let us underline that polydomain states of ferroelectric films are used in several classical and advanced applications. There are a lot of applications of periodically poled ferroelectric layers of different compositions, for instance $LiNbO_3$ [85], $LiTaO_3$ [86] and $KTiOPO_4$ [87], for phase-matching of the second and higher harmonic generation in nonlinear optic devices. 2D-semiconductors (e.g. graphene) placed on ferroelectric substrates with a domain structure are promising candidates in advanced memory cells, where each domain wall triggers the conductivity of the channel that is a 2D-semiconductor (see e.g. experimental works [88, 89, 90] and a recent theory [91, 92]. Hence, the revealed polydomain state in ultra-thin ferroelectric films induced by the flexo-chemical coupling can be of particular importance in advanced applications.

IV. CONCLUSIONS

Using Landau-Ginzburg-Devonshire approach we established the effect of the flexoelectro-chemical coupling on the polar properties and phase transitions in thin ferroelectric films with a surface layer of uncharged elastic point defects (vacancies or ions). We considered a typical case, when the defects are concentrated in a thin layer below the top film surface creating a sharp gradient of elastic fields. The defective surface of the film is not covered with an electrode, but with an ultra-thin layer of ambient screening charges, which are characterized by a surface screening length.

We obtained that the influence of the flexoelectro-chemical coupling and surface screening length on the ferroelectric transition temperature of the film, distribution of the spontaneous polarization and elastic fields, domain wall structure and period is rather strong, namely, it turned out that:

1. The screening length strongly affects the polar properties and domain structure in the film. In particular, a pronounced minimum appears on the dependence of the system's specific energy on the domain size with an increase of the screening length, the depth of the minimum depending essentially on the magnitude of the Vegard coefficient.
2. Due to the flexoelectric effect there is no size-induced transition to a paraelectric phase until (2 – 4) nm thickness of $PbTiO_3$ films with 1% of compressive misfit strain. The origin of this phenomenon is the re-building of the domain structure in the film (namely the cross-over from *c*-domain stripes to *a*-type closure domains) emerging with its thickness decrease below 4 nm, conditioned by the flexoelectric coupling and facilitated by negative Vegard coefficient. Though we observe no phase transition for smaller thickness, our results (as obtained in the continuum theory framework) can be inaccurate below the (2-4) nm size. Despite the said limitation the obtained results point at tempting opportunities for defect-strain engineering of the ultra-thin perovskite film ferroelectric properties and domain structure tuning, which can be very promising for the ferroic film applications in nanoelectronics.
3. Electric field induced by the defect layer has an unexpectedly strong influence on the polar and elastic properties of the strained films due to the coupling of inhomogeneous Vegard stresses and the flexoelectric effect (defect-driven flexo-chemical effect). Positive Vegard coefficients and high concentration of elastic defects effectively maintain the ferroelectric transition temperature above 350 K in the strained $PbTiO_3$ films due to the flexo-chemical effect. In contrast to the pure flexoelectric effect coefficients, which values are material-specific constants, the magnitude of the flexo-chemical effect can be controlled by the concentration of defects, their type and distribution in the film, making the considered system much more suitable for tuning.

4. The increase of defect concentration leads to a noticeable monotonic decrease in the ferroelectric transition temperature of the $PbTiO_3$ film with negative Vegard coefficients. In contrast, for positive Vegard coefficients, a pronounced maximum (with a height up to 200 K) appears on the thickness dependence of the transition temperature with increasing defect concentration. The film thickness corresponding to the maximum is approximately equal to the thickness of the defect layer and relatively weakly depends on the surface screening length. The latter property may have important implications for miniaturization of ferroelectric devices.
5. The pronounced maximum on the dependence of the ferroelectric transition temperature on the film thickness exists even without the flexoelectric coupling in the film, however, the coupling strongly shifts the transition temperature (by up to 30 K for thin $PbTiO_3$ films). Since the maximum position and height can be controlled by modifying the defect concentration and Vegard coefficient, the obtained results are promising for advanced applications in ferroelectric memory devices and those applications in nanoelecronics, where introducing of different types and amounts of defects is conceivable.

Acknowledgements

S.V.K study was supported by the U.S. DOE, Office of Basic Energy Sciences (BES), Materials Sciences and Engineering Division (MSED) under FWP Grant No. A portion of this research was conducted at the Center for Nanophase Materials Sciences, which is a DOE Office of Science User Facility. I.S.V. gratefully acknowledges support from the Deutsche Forschungsgemeinschaft (DFG) through the grant GE 1171/7-1.

Authors contribution

E.A.E. wrote the codes and, assisted by I.S.V. and E.N.F., performed numerical calculations. A.N.M. stated the problem and wrote the manuscript draft. E.A.E. and I.S.V. prepared the figures. Results analyses and manuscript improvement was performed by Y.A.G., M.D.G. and S.V.K.

APPENDIX

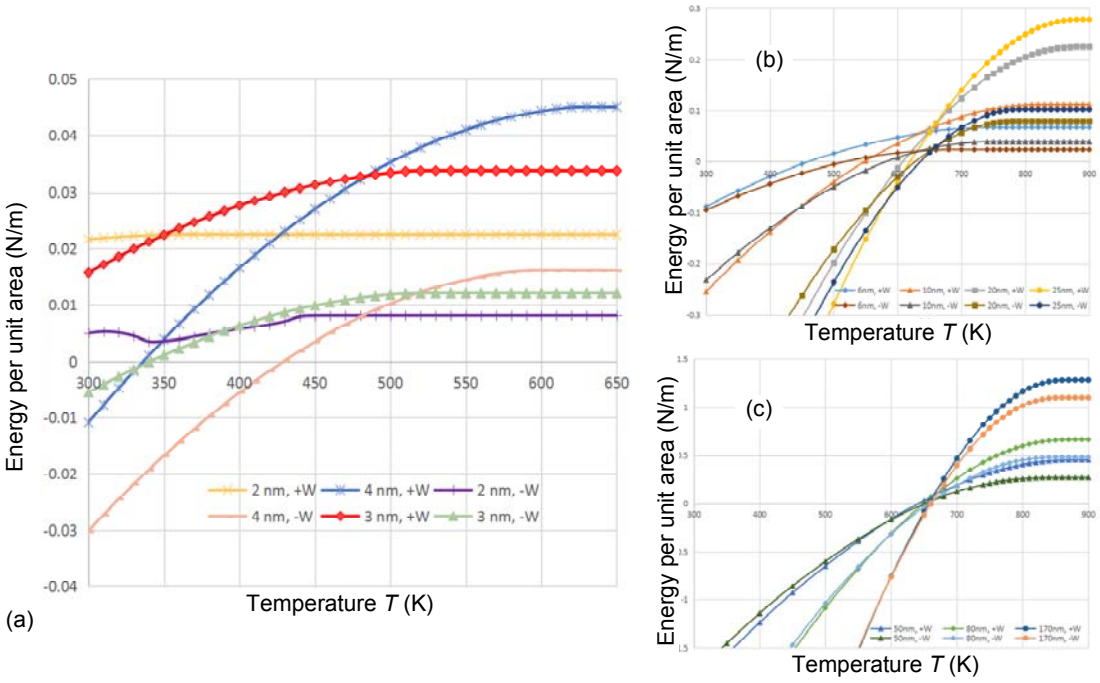

FIG. A1. Temperature-dependent energy diagram for the total energy in the thin films of thickness 2, 3 and 4 nm (a), 6, 10, 20 and 25 nm (b), 50, 80, 170 nm (c) with the defect concentration N_0=3×10^{26} 1/m³, h_0=25 nm, Δh=1 nm, λ=0.1 nm, at the room temperature (300 K), and the positive (W=+10 Å) and negative (W=-10 Å) Vegard coefficients. Saturation plateaus on the curves correspond to the paraelectric phase. Linear or parabolic-like dependencies correspond to the ferroelectric phase in the vicinity of respectively I and II-type phase transition. Note that the total energy of the system is greater than zero because of its mechanical component modified by a misfit strain.

REFERENCES

1 James F. Scott, *Ferroelectric Memories,* Springer Series in Advanced Microelectronics. Vol. 3 (2000). ISBN: 978-3-540-66387-4.

2 D.R. Tilley. *Finite-size effects on phase transitions in ferroelectrics. Ferroelectic Thin Films*. ed. C. Paz de Araujo, J.F. Scott and G.W. Teylor. (Amsterdam: Gordon and Breach, 1996).

3 M.J. Highland, T.T. Fister, D.D. Fong, P.H. Fuoss, C. Thompson, J.A. Eastman, S.K. Streiffer, and G.B. Stephenson. Equilibrium Polarization of Ultrathin PbTiO3 with Surface Compensation Controlled by Oxygen Partial Pressure, Phys. Rev. Lett. **107**, 187602 (2011).

4 I. Vrejoiu, G. Le Rhun, L. Pintilie, D. Hesse, M. Alexe, and U. Gösele. "Intrinsic ferroelectric properties of strained tetragonal PbZr0. 2Ti0. 8O3 obtained on layer–by–layer grown, defect–free single–crystalline films." Adv. mater. **18**, 1657 (2006).

5 D.D. Fong, G.B. Stephenson, S.K. Streiffer, J.A. Eastman, O. Auciello, P.H. Fuoss, and C. Thompson, Ferroelectricity in Ultrathin Perovskite Films, Science **304**, 1650 (2004).

[6] A. L. Roytburd, S. P. Alpay, V. Nagarajan, C. S. Ganpule, S. Aggarwal, E. D. Williams, and R. Ramesh. "Measurement of internal stresses via the polarization in epitaxial ferroelectric films." Phys. Rev. Lett. **85**, 190, (2000)

7 J. S. Speck, A. Seifert, W. Pompe, and R. Ramesh. "Domain configurations due to multiple misfit relaxation mechanisms in epitaxial ferroelectric thin films. II. Experimental verification and implications." J. Appl. Phys. **76**, 477 (1994).

8 N.A. Pertsev, A.G. Zembilgotov, and A.K. Tagantsev, Effect of Mechanical Boundary Conditions on Phase Diagrams of Epitaxial Ferroelectric Thin Films, Phys. Rev. Lett. **80**, 1988 (1998).

9 S.M. Kogan, Piezoelectric effect during inhomogeneous deformation and acoustic scattering of carriers in crystals, Sov. Phys. Solid State **5**, 2069 (1964).

10 N.D. Sharma, C. M. Landis, and P. Sharma. "Piezoelectric thin-film superlattices without using piezoelectric materials". J. Appl. Phys. **108**, 024304 (2010).

11 P. Zubko, G. Catalan, and A.K. Tagantsev, "Flexoelectric effect in solids," Annu. Rev. Mater. Res. **43**, 387 (2013).

12 M. Stengel, Flexoelectricity from density-functional perturbation theory. Phys. Rev. B **88**, 174106 (2013)

13 A.K. Tagantsev, and P.V. Yudin, eds. *Flexoelectricity in Solids: From Theory to Applications*. World Scientific, Singapore, 2016

14 D.A. Freedman, D. Roundy, and T.A. Arias, "Elastic effects of vacancies in strontium titanate: Short-and long-range strain fields, elastic dipole tensors, and chemical strain," Phys. Rev. B **80**, 064108 (2009).

15 G. Catalan and James F. Scott. "Physics and applications of bismuth ferrite." Adv. Mater. **21**, 1–23 (2009).

16 X. Zhang, W. Shyy, and A.M. Sastry, "Numerical simulation of intercalation-induced stress in Li-ion battery electrode particles." J. Electrochem. Soc., **154**, A910 (2007).

17 X. Zhang, A. M. Sastry, and W. Shyy, "Intercalation-induced stress and heat generation within single lithium-ion battery cathode particles." J. Electrochem. Soc., **155**, A542 (2008).

18 A.N. Morozovska, E.A. Eliseev, A.K. Tagantsev, S.L. Bravina, Long-Qing Chen, and S.V. Kalinin. Thermodynamics of electromechanically coupled mixed ionic-electronic conductors: Deformation potential, Vegard strains, and flexoelectric effect. Phys. Rev. B **83**, 195313 (2011).

19 A.N. Morozovska, I.S. Golovina, S.V. Lemishko, A.A. Andriiko, S.A. Khainakov, and E.A. Eliseev. Effect of Vegard strains on the extrinsic size effects in ferroelectric nanoparticles. Phys. Rev. B **90**, 214103 (2014)

20 A.N. Morozovska, E.A. Eliseev, P.S. Sankara Rama Krishnan, A. Tselev, E. Strelkov, A. Borisevich, O.V. Varenyk, N.V. Morozovsky, P. Munroe, S.V. Kalinin, and V. Nagarajan, "Defect thermodynamics and kinetics in thin strained ferroelectric films: The interplay of possible mechanisms." Phys. Rev. B **89**, 054102 (2014).

21 A.N. Morozovska, and M.D. Glinchuk. "Flexo-chemo effect in nanoferroics as a source of critical size disappearance at size-induced phase transitions." J. Appl. Phys. **119**, 094109 (2016).

22 J. Zhu, W. Han, H. Zhang, Z. Yuan, X-H. Wang, L-T. Li, and C-Q. Jin, Phase coexistence evolution of nano BaTiO3 as function of particle sizes and temperatures, J. Appl. Phys. **112**, 064110 (2012).

23 M. Marvan, ,P. Chvosta, and J. Fousek. "Theory of compositionally graded ferroelectrics and pyroelectricity." Appl. Phys. Lett. **86**, 221922 (2005).
24 A.L. Roytburd and J. Slutsker. “Thermodynamics of polydomain ferroelectric bilayers and graded multilayers” Appl. Phys. Lett. 89, 042907 (2006)
25 R. Kretschmer and K.Binder, Surface effects on phase transition in ferroelectrics and dipolar magnets. Phys. Rev. B. 20, 1065 (1979).
26 A.L. Roytburd, V. Roytburd, and J. Slutsker. “Domain structures in continuously graded ferroelectric films” Appl. Phys. Lett. 94, 152904 (2009)
27 A. Roytburd, V. Roytburd, Domain evolution and polarization of continuously graded ferroelectric films. Philosophical Magazine, **90**, 61–69 (2010).
[28] Y. L. Tang, Y. L. Zhu, X. L. Ma, A. Y. Borisevich, A. N. Morozovska, E. A. Eliseev, W. Y. Wang Y. J. Wang, Y. B. Xu, Z. D. Zhang, S. J. Pennycook. Observation of a periodic array of flux-closure quadrants in strained ferroelectric PbTiO3 films. Science **348**, no. 6234, 547-551 (2015)
[29] Nina Balke, Benjamin Winchester, Wei Ren, Ying Hao Chu, Anna N. Morozovska, Eugene A. Eliseev, Mark Huijben, Rama K. Vasudevan, Petro Maksymovych, Jason Britson, Stephen Jesse, Igor Kornev, Ramamoorthy Ramesh, Laurent Bellaiche, Long Qing Chen, and Sergei V. Kalinin. Enhanced electric conductivity at ferroelectric vortex cores in $BiFeO_3$. Nature Physics **8**, 81–88 (2012).
30 B. Winchester, N. Balke, X. X. Cheng, A. N. Morozovska, S. Kalinin, and L. Q. Chen. "Electroelastic fields in artificially created vortex cores in epitaxial $BiFeO_3$ thin films." *Applied Physics Letters* **107**, 052903 (2015).
31 A. R.Damodaran, J. D. Clarkson, Z. Hong, H. Liu, A. K. Yadav, C. T. Nelson, S-L. Hsu et al. "Phase coexistence and electric-field control of toroidal order in oxide superlattices." *Nature materials* 16 (2017): 1003.
32 A.M. Bratkovsky, and A.P. Levanyuk. "Smearing of phase transition due to a surface effect or a bulk inhomogeneity in ferroelectric nanostructures." Phys. Rev. Lett, **94**, 107601 (2005).
33 Z-G. Ban, S. P. Alpay, and J. V. Mantese. "Fundamentals of graded ferroic materials and devices." Phys. Rev. B **67**, 184104 (2003).
34 S. Zhong, Z-G. Ban, S.P. Alpay, and J.V. Mantese. "Large piezoelectric strains from polarization graded ferroelectrics." Appl. Phys. Lett. **89**, 142913 (2006).
35 A.N. Morozovska, E.A. Eliseev, G.S. Svechnikov, and S.V. Kalinin. "Mesoscopic mechanism of the domain wall interaction with elastic defects in uniaxial ferroelectrics." J. Appl. Phys. **113**, 187203 (2013).
36 I.S. Vorotiahin, A.N. Morozovska, E.A. Eliseev, Y.A. Genenko. Flexocoupling impact on the kinetics of polarization reversal. Phys. Rev. B **95**, 014104 (2017)
37 I.S. Vorotiahin, E.A. Eliseev, Q. Li, S.V. Kalinin, Y.A. Genenko and A.N. Morozovska. “Tuning the Polar States of Ferroelectric Films via Surface Charges and Flexoelectricity.” Acta Mater. **137,** 85 (2017).
38 G Catalan, L J Sinnamon, J M Gregg. The effect of flexoelectricity on the dielectric properties of inhomogeneously strained ferroelectric thin films. J. Phys.: Condens. Matter 16, 2253 (2004)
39 J. Karthik, R.V.K. Mangalam, J.C. Agar, and L.W. Martin. "Large built-in electric fields due to flexoelectricity in compositionally graded ferroelectric thin films." Phys.Rev. B **87**, 024111 (2013).

40 A.N. Morozovska, E.A. Eliseev, Y.A. Genenko, I.S. Vorotiahin, M.V. Silibin, Y. Cao, Y. Kim, M.D. Glinchuk, and S.V. Kalinin. "Flexocoupling impact on size effects of piezoresponse and conductance in mixed-type ferroelectric semiconductors under applied pressure." Phys. Rev. B **94**, 174101 (2016).
41 A. M. Bratkovsky, A. P. Levanyuk. "Formation and rapid evolution of domain structure at phase transitions in slightly inhomogeneous ferroelectrics and ferroelastics." Phys. Rev. B 66, 184109 (2002)
42 A.K. Tagantsev, L. E. Cross, and J. Fousek. *Domains in ferroic crystals and thin films*. New York: Springer, 2010.
43 A. L. Roytburd, Jun Ouyang, and Andrei Artemev. "Polydomain structures in ferroelectric and ferroelastic epitaxial films." J. Phys.: Condens. Matter **29**, 163001 (2017)
44 A.M. Bratkovsky, and A. P. Levanyuk. "Very large dielectric response of thin ferroelectric films with the dead layers." Phys. Rev. B 63, 132103 (2001).
45 A.K. Tagantsev and G. Gerra. "Interface-induced phenomena in polarization response of ferroelectric thin films." J. Appl. Phys. **100**, 051607 (2006).
46 E.A. Eliseev, A.N. Morozovska, M.D. Glinchuk, and R. Blinc, Spontaneous flexoelectric/flexomagnetic effect in nanoferroics, Phys. Rev. B. **79**, 165433 (2009).
47 P.V. Yudin, R. Ahluwalia, A.K. Tagantsev. Upper bounds for flexocoupling coefficients in ferroelectrics, Appl. Phys. Lett. **104**(8), 082913 (2014)
48 E.A. Eliseev, A.V. Semchenko, Y.M. Fomichov, M. D. Glinchuk, V.V. Sidsky, V.V. Kolos, Y.M. Pleskachevsky, M.V. Silibin, N.V. Morozovsky, A.N. Morozovska. Surface and finite size effects impact on the phase diagrams, polar and dielectric properties of $(Sr,Bi)Ta_2O_9$ ferroelectric nanoparticles. J. Appl. Phys. **119**, 204104 (2016)
49 J. Bardeen, "Surface states and rectification at a metal semi-conductor contact." Phys. Rev. **71**, 717 (1947).
50 V.M. Fridkin, *Ferroelectrics semiconductors*, Consultant Bureau, New-York and London (1980). p. 119.
51 M.A. Itskovsky, "Some peculiarities of phase transition in thin layer ferroelectric." Fiz. Tv. Tela **16**, 2065 (1974).
52 P.W.M. Blom, R.M. Wolf, J.F.M. Cillessen, and M.P.C.M. Krijn. "Ferroelectric Schottky diode." Phys. Rev. Lett. **73**, 2107 (1994).
53A.N. Morozovska, E.A. Eliseev, S.V. Svechnikov, A.D. Krutov, V.Y. Shur, A.Y. Borisevich, P. Maksymovych, and S.V. Kalinin. ”Finite size and intrinsic field effect on the polar-active properties of ferroelectric semiconductor heterostructures.” Phys. Rev. B. **81**, 205308 (2010).
54 Y.A. Genenko, O. Hirsch, and P. Erhart, “Surface potential at a ferroelectric grain due to asymmetric screening of depolarization fields.” J. Appl. Phys. **115**, 104102 (2014).
55 J. Wang, A.K. Tagantsev, and N. Setter. "Size effect in ferroelectrics: Competition between geometrical and crystalline symmetries" Phys. Rev. **B 83**, 014104 (2011).
56 R. Maranganti and P. Sharma, A novel atomistic approach to determination of strain-gradient elasticity constants: Tabulation and comparison for various metals, semiconductors, silica, polymers and the (ir) relevance for nanotechnologies, J. Mech. Phys. Solids **55**, 1823 (2007)

57 A.S. Yurkov, “Elastic boundary conditions in the presence of the flexoelectric effect”. JETP Letters **94** (6), 455 (2011).
58 Flexoelectricity in Solids: From Theory to Applications. Ed. by A.K. Tagantsev and P.V. Yudin, World Scientific (2016)] and Refs. Therein.
59 P.V. Yudin, A.K. Tagantsev, E.A. Eliseev, A.N. Morozovska and N. Setter. “Bichiral structure of ferroelectric domain walls driven by flexoelectricity”. Phys. Rev. B **86**, 134102 (2012).
60 E.A. Eliseev, P.V. Yudin, S.V. Kalinin, N. Setter, A.K. Tagantsev and A.N. Morozovska. “Structural phase transitions and electronic phenomena at 180-degree domain walls in rhombohedral BaTiO3”. Phys. Rev. B **87**, 054111 (2013).
61 P.V. Yudin, R. Ahluwalia, A.K. Tagantsev. ”Upper bounds for flexocoupling coefficients in ferroelectrics”. Appl. Phys. Lett. **104**, 082913 (2014).
62 A.N. Morozovska, E.A. Eliseev, C.M. Scherbakov, and Y.M. Vysochanskii. “The influence of elastic strain gradient on the upper limit of flexocoupling strength, spatially-modulated phases and soft phonon dispersion in ferroics”. Phys. Rev. **B** 94, 174112 (2016).
63 Exactly these conditions correspond to the minimum of the Gibbs potential, see §10 in L.D. Landau and E.M. Lifshitz, Theoretical Physics, Electrodynamics of Continuous Media, Vol. VIII, Pergamon, Oxford, 1963.
64 Eugene A. Eliseev, Anna N. Morozovska. General approach for the description of size effects in ferroelectric nanosystems. J Mater. Sci. 44, 5149–5160 (2009).
[65] Eugene A. Eliseev, Sergei V. Kalinin, Anna N. Morozovska. Finite size effects in ferroelectric-semiconductor thin films under open-circuited electric boundary conditions. Journal of Applied Physics 117, 034102 (2015)
66. B.W. Sheldon, V.B. Shenoy, Space charge induced surface stresses: implications in ceria and other ionic solids, Phys. Rev. Lett. **106**, 216104 (2011).
67 P. Erhart, and K. Albe. "Dopants and dopant–vacancy complexes in tetragonal lead titanate: A systematic first principles study." Comput. Mater. Sci. 103, 224 (2015).
68 B. Jaffe, W.R. Cook and H. Jaffe, Piezoelectric Ceramics. Academic Press, London and New York, 1971.
69 J.K. Juneja, S. Singh, K.K. Raina, C. Prakash, Study on structural, dielectric, ferroelectric and piezoelectric properties of Ba doped Lead Zirconate Titanate Ceramics, Physica B: Condensed Matter 431, 109 (2013)
70 D.M. Nguyen, T.Q. Trinh, J.M. Dekkers, E.P. Houwman, H.N. Vu, A.J.H.M. Rijnders, Effect of dopants on ferroelectric and piezoelectric properties of lead zirconate titanate thin films on Si substrates, Ceramics international 40, 1013 (2014)
71 J.-B. Liu, W.-C. Li, Y.-X. Zhang, and Z.-M. Wang. "Preparation and characterization of Li+-modified $Ca_xPb_{1-x}TiO_3$ film for humidity sensor." Sens. Actuators B: Chem. 75, 11 (2001).
72 Aneta Slodczyk, Marie-Hélène Limage, Philippe Colomban, Oumaya Zaafrani, Frédéric Grasset, Johan Loricourt, and Béatrice Sala. "Substitution and proton doping effect on SrZrO3 behaviour: high-pressure Raman study." *J. Raman Spectrosc.* 42, 2089 (2011).
73 K. Wójcik. Electrical properties of PbTiO3 single crystals doped with lanthanum, Ferroelectrics, 99:1, 5 (1989).

74 I. Ueda, and S. Ikegami. "Piezoelectric properties of modified PbTiO3 ceramics." Jpn. J. Appl. Phys. 7, 236 (1968).

75 R. Maranganti and P. Sharma. "Atomistic determination of flexoelectric properties of crystalline dielectrics" Phys. Rev. B **80**, 054109 (2009).

76J.W. Hong and D. Vanderbilt, "First-principles theory and calculation of flexoelectricity", Phys. Rev. B **88**, 174107 (2013).

77 M. Stengel, "Unified ab initio formulation of flexoelectricity and strain-gradient elasticity", Phys. Rev. B **93**, 245107 (2016).

78 I. Ponomareva, A.K. Tagantsev, and L. Bellaiche. "Finite-temperature flexoelectricity in ferroelectric thin films from first principles". Phys. Rev B **85**, 104101 (2012).

79 P. Zubko, G. Catalan, A. Buckley, P.R.L. Welche, and J.F. Scott. "Strain-Gradient-Induced Polarization in SrTiO3 Single Crystals". Phys. Rev. Lett. **99**, 167601 (2007).

80 P. Zubko, G. Catalan, A. Buckley, P.R.L. Welche, and J.F. Scott. Erratum: "Strain-Gradient-Induced Polarization in SrTiO3 Single Crystals" [Phys. Rev. Lett. **99**, 167601(2007)]**.** Phys. Rev. Lett. **100,** 199906 (2008).

81 W. Ma and L.E. Cross, "Flexoelectric effect in ceramic lead zirconate titanate". Appl. Phys. Lett. **86**, 072905 (2005).

82 R.von Mises,. *Mechanik der festen Körper im plastisch deformablen Zustand.* Göttin. Nachr. Math. Phys., **1**, pp. 582. (1913), see also https://en.wikipedia.org/wiki/Von_Mises_yield_criterion

83 E.A. Eliseev, A.N. Morozovska, S.V. Kalinin, Y.L. Li, Jie Shen, M.D. Glinchuk, L.Q. Chen, V. Gopalan. Surface Effect on Domain Wall Width in Ferroelectrics. J. Appl. Phys. **106**, 084102 (2009).

84 A.S. Sidorkin. Domain Structure in Ferroelectrics and Related Materials. Cambridge Int Science Publishing, 2006 - 250 pp.

85 R. G., Batchko, M. M. Fejer, R.L. Byer, D. Woll, R. Wallenstein, V. Y. Shur, and L. Erman. "Continuous-wave quasi-phase-matched generation of 60 mW at 465 nm by single-pass frequency doubling of a laser diode in backswitch-poled lithium niobate." Opt. Lett. 24, 1293 (1999).

86 H. Takaaki, K. Nakamura, T. Taniuchi, H. Ito, Y. Furukawa, and K. Kitamura. "Quasi-phase-matched optical parametric oscillation with periodically poled stoichiometric $LiTaO_3$." Opt. Lett. 25, 651 (2000).

87 A. Garashi, A. Arie, A. Skliar, and G. Rosenman. "Continuous-wave optical parametric oscillator based on periodically poled KTiOPO 4." Opt. Lett. 23, 1739 (1998).

88 J. H. Hinnefeld, R.-J. Xu, S. Rogers, S. Pandya, M. Shim, L. W. Martin, N. Mason. "Single Gate PN Junctions in Graphene-Ferroelectric Devices." *arXiv preprint arXiv:1506.07138* (2015)

89 C. Baeumer, D. Saldana-Greco, J. M. P. Martirez, A. M. Rappe, M. Shim, L. W. Martin. "Ferroelectrically driven spatial carrier density modulation in graphene." Nat. Commun. **6**, 6136 (2015)

90 W. Y. Kim, H.-D. Kim, T.-T. Kim, H.-S. Park, K.H. Lee, H. J. Choi, S. H. Lee, J.-H. Son, N.-K. Park, and B.K. Min. "Graphene-ferroelectric metadevices for nonvolatile memory and reconfigurable logic-gate operations." Nat. Commun. **7**, 10429 (2016)

91 Anatolii I. Kurchak, Eugene A. Eliseev, Sergei V. Kalinin, Maksym V. Strikha, and Anna N. Morozovska. P-N junctions dynamics in graphene channel induced by ferroelectric domains motion. Phys. Rev. Applied **8**, 024027 (2017)

92 Anna N. Morozovska, Anatolii I. Kurchak, and Maksym V. Strikha. Graphene exfoliation at ferroelectric domain wall induced by piezoeffect: impact on the conduction of graphene channel Phys. Rev. Applied **8**, 054004 (2017)